

Grid-less Variational Bayesian Inference of Line Spectral from Quantized Samples

Jiang Zhu, Qi Zhang and Xiangming Meng

Abstract

Efficient estimation of line spectral from quantized samples is of significant importance in information theory and signal processing, e.g., channel estimation in energy efficient massive MIMO systems and direction of arrival estimation. The goal of this paper is to recover the line spectral as well as its corresponding parameters including the model order, frequencies and amplitudes from heavily quantized samples. To this end, we propose an efficient grid-less Bayesian algorithm named VALSE-EP, which is a combination of the variational line spectral estimation (VALSE) and expectation propagation (EP). The basic idea of VALSE-EP is to iteratively approximate the challenging quantized model of line spectral estimation as a sequence of simple pseudo unquantized models so that the VALSE can be applied. Note that the noise in the pseudo linear model is heteroscedastic, i.e., different components having different variances, and a variant of the VALSE is re-derived to obtain the final VALSE-EP. Moreover, to obtain a benchmark performance of the proposed algorithm, the Cramér Rao bound (CRB) is derived. Finally, numerical experiments on both synthetic and real data are performed, demonstrating the near CRB performance of the proposed VALSE-EP for line spectral estimation from quantized samples.

Keywords: Variational Bayesian inference, expectation propagation, quantization, line spectral estimation, MMSE, gridless

I. INTRODUCTION

Line spectral estimation (LSE) is a fundamental problem in information theory and statistical signal processing which has widespread applications, e.g., channel estimation [2], direction of arrival (DOA) estimation [3]. To address this problem, on one hand, many classical methods have been proposed, such as the fast Fourier transform (FFT) based periodogram [4], subspace based MUSIC [5] and ESPRIT [6]. On the other hand, to exploit the frequency sparsity of the line spectral signal, sparse representation

Jiang Zhu and Qi Zhang are with the Key Laboratory of Ocean Observation-imaging Testbed of Zhejiang Province, Ocean College, Zhejiang University, No.1 Zheda Road, Zhoushan, 316021, China. Xiangming Meng is with Huawei Technologies, Co. Ltd., Shanghai, 201206, China.

and compressed sensing (CS) based methods have been proposed to estimate frequencies for multiple sinusoids.

Depending on the model adopted, CS based methods for LSE can be classified into three categories, namely, on-grid, off-grid and grid-less, which also correspond to the chronological order in which they have been developed [7]. At first, on-grid methods where the continuous frequency is discretized into a finite set of grid points are proposed [8]. It is shown that grid based methods will incur basis mismatch when the true frequencies do not lie exactly on the grid [9]. Then, off-grid compressed sensing methods have been proposed. In [10], a Newtonalized orthogonal matching pursuit (NOMP) method is proposed, where a Newton step and feedback are utilized to refine the frequency estimates. Compared to the incremental step in updating the frequencies in NOMP, the iterative reweighted approach (IRA) [11] estimates the frequencies in parallel, which improves the estimation accuracy at the cost of increasing complexity. In [12], superfast LSE method is proposed based on fast Toeplitz matrix inversion algorithm. In [13, 14], a sparse Bayesian learning method is proposed, where the grid bias and the grid are jointly estimated [13], or the Newton method is applied to refine the frequency estimates [14]. To completely overcome the grid mismatch problem, grid-less based methods have been proposed [15–18]. The atomic norm-based methods involve solving a semidefinite programming (SDP) problem [19], whose computation complexity is prohibitively high for large problem size. In [20], a grid-less variational line spectral estimation (VALSE) algorithm is proposed, where posterior probability density function (PDF) of the frequency is provided. In [21], the multisnapshot VALSE (MVALSE) is developed for the MMVs setting, which also shows the relationship between the VALSE and the MVALSE.

In practice, the measurements might be obtained in a nonlinear way, either preferably or inevitably. For example, in the mmWave multiple input multiple output (MIMO) system, since the mmWave accompanies large bandwidths, the cost and power consumption are huge due to high precision (e.g., 10-12 bits) analog-to-digital converters (ADCs) [22]. Consequently, low precision ADCs (often 1 – 3 bits) are adopted to alleviate the ADC bottleneck. Another motivation is wideband spectrum sensing in bandwidth-constrained wireless networks [23, 24]. In order to reduce the communication overhead, the sensors quantize their measurements into a single bit, and the spectrum is estimated from the heavily quantized measurements at the fusion center (FC). There are also various scenarios where measurements are inevitably obtained nonlinearly such as phase retrieval [25, 26]. As a result, it is of great significance in designing efficient nonlinear LSE algorithms. This paper will consider in particular LSE from low precision quantized observations [27, 28] but extension to general nonlinear scenarios could easily fit into our proposed framework without much difficulty.

A. Related Work

Many classical methods have been extended to solve the LSE from quantized samples. In [29], the spectrum of the one-bit data is analyzed, which consists of plentiful harmonics. It shows that under low signal to noise ratio (SNR) scenario, the amplitudes of the higher order harmonics are much smaller than that of the fundamental frequency, thus the classical FFT based method still works well for the SAR imaging experiment. However, the FFT based method can overestimate the model order (number of spectrums) in the high SNR scenario. As a consequence, the quantization effects must be taken into consideration. The CS based methods have been proposed to solve the LSE from quantized samples, which can also be classified into on-grid, off-grid and grid-less methods.

- on-grid methods: The on-grid methods can be classified into l_1 minimization based approach [30–32] and generalized sparse Bayesian learning (Gr-SBL) [33] algorithm. For l_1 minimization approach, the regularization parameter is hard to determine the tradeoff between the fitting error and the sparsity. While the reconstruction accuracy of the Gr-SBL is high, its computation complexity is high since it involves a matrix inversion in each iteration.
- off-grid methods: The SVM based [34] and 1bRelax algorithm [35] are two typical approaches. For the SVM based approach, the model order needs to be known a priori, while the 1bRelax algorithm [36] get rid of such need by using the consistent Bayesian information criterion (BIC) to determine the model order.
- grid-less methods: The grid-less approach can completely overcome the grid mismatch problem and the atomic norm minimization approach has been proposed [37–39]. However, its computational complexity is high as it involves solving a SDP.

From the point of view of CS, many Bayesian algorithms have been developed, such as approximate message passing (AMP) [43, 44], vector AMP (VAMP) [48]. It is shown in [45, 46] that AMP can be alternatively derived via expectation propagation (EP) [40], an effective approximate Bayesian inference method. To deal with nonlinear observations, i.e., generalized linear models (GLM), AMP and VAMP are extended to GAMP [47] and GVAMP [49] respectively using different methods. The authors in [41] propose a unified Bayesian inference framework for the GLM inference which shows that GLM could be iteratively approximated as a standard linear model (SLM) using EP¹. This unified framework provides new insights into some existing algorithms, as elucidated by a concise derivation of GAMP in [41], and motivates the design of new algorithms such as the generalized SBL (Gr-SBL) algorithm [33, 41]. This paper extends the idea further and utilize EP to solve LSE from quantized samples.

¹The extrinsic message in [41] could be equivalently obtained through EP.

B. Main Contributions

This work studies the LSE problem from quantized measurements. Utilizing the EP [40], the generalized linear model can be iteratively decomposed as two modules (a standard linear model ² and a componentwise minimum mean squared error (MMSE) module) [41]. Thus the VALSE algorithm is run in the standard linear module where the frequency estimate is iteratively refined. For the MMSE module, it refines the pseudo observations of the linear model ³. By iterating between the two modules, the estimates of the frequency are improved gradually. The main contributions of this work are summarized as follows:

- A VALSE-EP method is proposed to deal with the LSE from quantized samples. The quantized model is iteratively approximated as a sequence of pseudo unquantized models with heteroscedastic noise (different components having different variance), a variant of the VALSE is re-derived.
- The VALSE-EP is a completely grid-less approach. Besides, the model order estimation is coupled within the iteration and the computational complexity is low, compared to the atomic norm minimization approach.
- The relationship between VALSE and VALSE-EP is revealed under the unquantized case. It is shown that the major difference lies in the noise variance estimation step. For VALSE-EP, it is iteratively solved by exchanging extrinsic information between the pseudo unquantized module (module A) and the MMSE module (module B). For VALSE, the noise variance estimate is equivalently derived through the expectation maximization (EM) step in module A, while VALSE-EP utilizes the EM step to estimate the noise variance in module B, which demonstrate that VALSE and VALSE-EP are not exactly equivalent.
- Utilizing the framework from [41], VALSE-EP is proposed which combines the VALSE algorithm with EP. The two different criteria are combined together, and numerical experiments on both synthetic and real data demonstrate the excellent performance of VALSE-EP.
- Although this paper focuses on the case of quantized measurements, it is believed that VALSE-EP can be easily extended to other nonlinear measurement scenarios such as phase retrieval without overcoming much difficulty.

²In fact, it is a nonlinear model instead of a standard linear model, which is different from [41] since the frequencies are unknown.

³Iteratively approximating the generalized linear model as a standard linear model is very beneficial, as many well developed methods such as the information-theoretically optimal successive interference cancellation (SIC) is developed in the SLM.

C. Paper Organization and Notation

The rest of this paper is organized as below. Section II describes the system model and introduces the probabilistic formulation. Section III derives the Cramér Rao bound (CRB). Section IV develops the VALSE for heterogenous noise. The VALSE-EP algorithm and the details of the updating expressions are presented in Section V. The relationship between VALSE and VALSE-EP in the unquantized setting is revealed in Section VI. Substantial numerical experiments are provided in Section VII and Section VIII concludes the paper.

For a complex vector $\mathbf{x} \in \mathbb{C}^M$, let $\Re\{\mathbf{x}\}$ and $\Im\{\mathbf{x}\}$ denote the real and imaginary part of \mathbf{x} , respectively, let $|\mathbf{x}|$ and $\angle\mathbf{x}$ denote the componentwise amplitude and phase of \mathbf{x} , respectively. For the square matrix \mathbf{A} , let $\text{diag}(\mathbf{A})$ return a vector with elements being the diagonal of \mathbf{A} . While for a vector \mathbf{a} , let $\text{diag}(\mathbf{a})$ return a diagonal matrix with the diagonal being \mathbf{a} , and thus $\text{diag}(\text{diag}(\mathbf{A}))$ returns a diagonal matrix. Let j denote the imaginary number. Let $\mathcal{S} \subset \{1, \dots, N\}$ be a subset of indices and $|\mathcal{S}|$ denote its cardinality. For the matrix $\mathbf{J} \in \mathbb{C}^{N \times N}$, let $\mathbf{J}_{\mathcal{S}}$ denote the submatrix by choosing both the rows and columns of \mathbf{J} indexed by \mathcal{S} . Similarly, let $\mathbf{h}_{\mathcal{S}}$ denote the subvector by choosing the elements of \mathbf{h} indexed by \mathcal{S} . Let $(\cdot)_{\mathcal{S}}^*$, $(\cdot)_{\mathcal{S}}^{\text{T}}$ and $(\cdot)_{\mathcal{S}}^{\text{H}}$ be the conjugate, transpose and Hermitian transpose operator of $(\cdot)_{\mathcal{S}}$, respectively. For the matrix \mathbf{A} , let $|\mathbf{A}|$ denote the elementwise absolute value of \mathbf{A} . Let \mathbf{I}_L denote the identity matrix of dimension L . “ $\sim i$ ” denotes the indices \mathcal{S} excluding i . Let $\mathcal{CN}(\mathbf{x}; \boldsymbol{\mu}, \boldsymbol{\Sigma})$ denote the complex normal distribution of \mathbf{x} with mean $\boldsymbol{\mu}$ and covariance $\boldsymbol{\Sigma}$. Let $\phi(x) = \exp(-x^2/2)/\sqrt{2\pi}$ and $\Phi(x) = \int_{-\infty}^x \phi(t)dt$ denote the standard normal probability density function (PDF) and cumulative distribution function (CDF), respectively. Let $\mathcal{W}(\cdot)$ wrap frequency in radians to the interval $[-\pi, \pi]$.

II. PROBLEM SETUP

Let $\mathbf{z} \in \mathbb{C}^N$ be a line spectra consisting of K complex sinusoids

$$\mathbf{z} = \sum_{k=1}^K \mathbf{a}(\tilde{\theta}_k) \tilde{w}_k, \quad (1)$$

where \tilde{w}_k is the complex amplitude of the k th frequency, $\tilde{\theta}_k \in [-\pi, \pi)$ is the k th frequency, and

$$\mathbf{a}(\theta) = [1, e^{j\theta}, \dots, e^{j(N-1)\theta}]^{\text{T}}. \quad (2)$$

The noisy measurements of \mathbf{z} are observed and quantized into a finite number of bits ⁴, i.e.,

$$\mathbf{y} = \mathcal{Q}(\Re\{\mathbf{z} + \boldsymbol{\epsilon}\}) + j\mathcal{Q}(\Im\{\mathbf{z} + \boldsymbol{\epsilon}\}), \quad (3)$$

⁴Extending to the incomplete measurement scenario where only a subset of measurements $\mathcal{M} = \{m_1, \dots, m_M\} \subseteq \{0, 1, \dots, N-1\}$ is observed is straightforward. For notation simplicity, we study the full measurement scenario. But the code that we have made available [1] does provide the required flexibility.

where $\epsilon \sim \mathcal{CN}(\epsilon; \mathbf{0}, \sigma^2 \mathbf{I}_N)$, σ^2 is the variance of the noise, $\mathcal{Q}(\cdot)$ is a quantizer which is applied componentwise to map the continuous values into discrete numbers. Specifically, let the quantization intervals be $\{(t_l, t_{l+1})\}_{l=0}^{|\mathcal{D}|-1}$, where $t_0 = -\infty$, $t_{\mathcal{D}} = \infty$, $\bigcup_{l=0}^{|\mathcal{D}|-1} [t_l, t_{l+1}) = \mathbb{R}$. Given a real number $a \in [t_l, t_{l+1})$, the representation is

$$\mathcal{Q}(a) = \omega_l, \quad \text{if } a \in [t_l, t_{l+1}). \quad (4)$$

Note that for a quantizer with bit-depth B , the cardinality of the output of the quantizer is $|\mathcal{D}| = 2^B$.

The goal of LSE is to jointly recover the number of spectrums \hat{K} (also named model order), the set of frequencies $\hat{\boldsymbol{\theta}} = \{\hat{\theta}_k\}_{k=1}^{\hat{K}}$, the corresponding coefficients $\{\hat{w}_k\}_{k=1}^{\hat{K}}$ and the LSE $\hat{\mathbf{z}} = \sum_{k=1}^{\hat{K}} \hat{\mathbf{a}}(\theta_k) \hat{w}_k$ from quantized measurements \mathbf{y} .

Since the sparsity level K is usually unknown, the line spectral consisting of N complex sinusoids is assumed [20]

$$\mathbf{z} = \sum_{i=1}^N w_i \mathbf{a}(\theta_i) \triangleq \mathbf{A}(\boldsymbol{\theta}) \mathbf{w}, \quad (5)$$

where $\mathbf{A}(\boldsymbol{\theta}) = [\mathbf{a}(\theta_1), \dots, \mathbf{a}(\theta_N)]$ and N satisfies $N > K$. Since the number of frequencies is K , the binary hidden variables $\mathbf{s} = [s_1, \dots, s_N]^T$ are introduced, where $s_i = 1$ means that the i th frequency is active, otherwise deactive ($w_i = 0$). The probability mass function (PMF) of s_i is

$$p(s_i; \rho) = \rho^{s_i} (1 - \rho)^{(1-s_i)}, \quad s_i \in \{0, 1\}. \quad (6)$$

Given that $s_i = 1$, we assume that $w_i \sim \mathcal{CN}(w_i; 0, \tau)$. Thus (s_i, w_i) follows a Bernoulli-Gaussian distribution, that is

$$p(w_i | s_i; \tau) = (1 - s_i) \delta(w_i) + s_i \mathcal{CN}(w_i; 0, \tau). \quad (7)$$

According to (6) and (7), the parameter ρ denotes the probability of the i th component being active and τ is a variance parameter. The variable $\boldsymbol{\theta} = [\theta_1, \dots, \theta_N]^T$ has the prior PDF $p(\boldsymbol{\theta}) = \prod_{i=1}^N p(\theta_i)$. Without any knowledge of the frequency θ_i , the uninformative prior distribution $p(\theta_i) = 1/(2\pi)$ is used [20]. For encoding the prior distribution, please refer to [20, 21] for further details.

Given \mathbf{z} , the PDF $p(\mathbf{y} | \mathbf{z}; \sigma^2)$ of \mathbf{y} can be easily calculated through (3). Let

$$\boldsymbol{\Omega} = (\theta_1, \dots, \theta_N, (\mathbf{w}, \mathbf{s})), \quad (8)$$

$$\boldsymbol{\beta} = \{\boldsymbol{\beta}_w, \boldsymbol{\beta}_z\}, \quad (9)$$

be the set of all random variables and the model parameters, respectively, where $\boldsymbol{\beta}_w = \{\rho, \tau\}$ and $\boldsymbol{\beta}_z = \{\sigma^2\}$. According to the Bayes rule, the joint PDF $p(\mathbf{y}, \mathbf{z}, \boldsymbol{\Omega}; \boldsymbol{\beta})$ is

$$p(\mathbf{y}, \mathbf{z}, \boldsymbol{\Omega}; \boldsymbol{\beta}) = p(\mathbf{y} | \mathbf{z}) \delta(\mathbf{z} - \mathbf{A}(\boldsymbol{\theta}) \mathbf{w}) \prod_{i=1}^N p(\theta_i) p(w_i | s_i) p(s_i). \quad (10)$$

Given the above joint PDF (10), the type II maximum likelihood (ML) estimation of the model parameters $\hat{\boldsymbol{\beta}}_{\text{ML}}$ is

$$\hat{\boldsymbol{\beta}}_{\text{ML}} = \underset{\boldsymbol{\beta}}{\operatorname{argmax}} p(\mathbf{y}; \boldsymbol{\beta}) = \underset{\boldsymbol{\beta}}{\operatorname{argmax}} \int p(\mathbf{y}, \mathbf{z}, \boldsymbol{\Omega}; \boldsymbol{\beta}) d\mathbf{z} d\boldsymbol{\Omega}. \quad (11)$$

Then the minimum mean squared error (MMSE) estimates of the parameters $(\mathbf{z}, \boldsymbol{\Omega})$ are

$$(\hat{\mathbf{z}}, \hat{\boldsymbol{\Omega}}) = \mathbb{E}[(\mathbf{z}, \boldsymbol{\Omega}) | \mathbf{y}; \hat{\boldsymbol{\beta}}_{\text{ML}}], \quad (12)$$

where the expectation is taken with respect to

$$p(\mathbf{z}, \boldsymbol{\Omega} | \mathbf{y}; \hat{\boldsymbol{\beta}}_{\text{ML}}) = \frac{p(\mathbf{z}, \boldsymbol{\Omega}, \mathbf{y}; \hat{\boldsymbol{\beta}}_{\text{ML}})}{p(\mathbf{y}; \hat{\boldsymbol{\beta}}_{\text{ML}})}. \quad (13)$$

Directly solving the ML estimate of $\boldsymbol{\beta}$ (11) or the MMSE estimate of $(\mathbf{z}, \boldsymbol{\Omega})$ (12) are both intractable. As a result, an iterative algorithm is designed in Section V.

III. CRAMÉR RAO BOUND

Before designing the recovery algorithm, the performance bounds of unbiased estimators are derived, i.e., the Cramér Rao bound (CRB). Although the Bayesian algorithm is designed, the CRB can be acted as the performance benchmark of the algorithm. To derive the CRB, K is assumed to be known, the frequencies $\tilde{\boldsymbol{\theta}} \in \mathbb{R}^K$ and weights $\tilde{\mathbf{w}} \in C^K$ are treated as deterministic unknown parameters, and the Fisher information matrix (FIM) $\mathbf{F}(\boldsymbol{\kappa})$ is calculated first. Let $\boldsymbol{\kappa}$ denote the set of parameters, i.e., $\boldsymbol{\kappa} = [\tilde{\boldsymbol{\theta}}^T, \tilde{\mathbf{g}}^T, \tilde{\boldsymbol{\phi}}^T]^T \in \mathbb{R}^{3K}$, where $\tilde{\mathbf{g}} = |\tilde{\mathbf{w}}|$ and $\tilde{\boldsymbol{\phi}} = \angle \tilde{\mathbf{w}}$. The PMF of the measurements $p(\mathbf{y} | \boldsymbol{\kappa})$ is

$$p(\mathbf{y} | \boldsymbol{\kappa}) = \prod_{n=1}^N p(y_n | \boldsymbol{\kappa}) = \prod_{n=1}^N p(\Re\{y_n\} | \boldsymbol{\kappa}) p(\Im\{y_n\} | \boldsymbol{\kappa}). \quad (14)$$

Moreover, the PMFs of $\Re\{y_n\}$ and $\Im\{y_n\}$ are

$$p(\Re\{y_n\} | \boldsymbol{\kappa}) = \prod_{\omega_l \in \mathcal{D}} p_{\Re\{y_n\}}(\omega_l | \boldsymbol{\kappa})^{\mathbb{I}_{\Re\{y_n\}=\omega_l}}, \quad (15)$$

$$p(\Im\{y_n\} | \boldsymbol{\kappa}) = \prod_{\omega_l \in \mathcal{D}} p_{\Im\{y_n\}}(\omega_l | \boldsymbol{\kappa})^{\mathbb{I}_{\Im\{y_n\}=\omega_l}}, \quad (16)$$

where $\mathbb{I}_{(\cdot)}$ is the indicator function,

$$p_{\Re\{y_n\}}(\omega_l | \boldsymbol{\kappa}) = \mathbb{P}(\Re\{z_n + \varepsilon_n\} \in [t_l, t_{l+1})) \quad (17a)$$

$$= \Phi\left(\frac{t_{l+1} - \Re\{z_n\}}{\sigma/\sqrt{2}}\right) - \Phi\left(\frac{t_l - \Re\{z_n\}}{\sigma/\sqrt{2}}\right), \quad (17b)$$

$$p_{\Im\{y_n\}}(\omega_l | \boldsymbol{\kappa}) = \mathbb{P}(\Im\{z_n + \varepsilon_n\} \in [t_l, t_{l+1})) \quad (17c)$$

$$= \Phi\left(\frac{t_{l+1} - \Im\{z_n\}}{\sigma/\sqrt{2}}\right) - \Phi\left(\frac{t_l - \Im\{z_n\}}{\sigma/\sqrt{2}}\right). \quad (17d)$$

The CRB is equal to the inverse of the FIM $\mathbf{F}(\boldsymbol{\kappa}) \in \mathbb{R}^{3K \times 3K}$

$$\mathbf{F}(\boldsymbol{\kappa}) = \mathbb{E} \left[\left(\frac{\partial \log p(\mathbf{y}|\boldsymbol{\kappa})}{\partial \boldsymbol{\kappa}} \right) \left(\frac{\partial \log p(\mathbf{y}|\boldsymbol{\kappa})}{\partial \boldsymbol{\kappa}} \right)^{\text{T}} \right]. \quad (18)$$

To calculate the FIM, the following Theorem [38] is utilized.

Theorem 1 [38] *The FIM $\mathbf{F}(\boldsymbol{\kappa})$ for estimating the unknown parameter $\boldsymbol{\kappa}$ is*

$$\begin{aligned} \mathbf{F}(\boldsymbol{\kappa}) = & \sum_{n=1}^N \left(\lambda_n \frac{\partial \Re\{z_n\}}{\partial \boldsymbol{\kappa}} \left(\frac{\partial \Re\{z_n\}}{\partial \boldsymbol{\kappa}} \right)^{\text{T}} \right. \\ & \left. + \chi_n \frac{\partial \Im\{z_n\}}{\partial \boldsymbol{\kappa}} \left(\frac{\partial \Im\{z_n\}}{\partial \boldsymbol{\kappa}} \right)^{\text{T}} \right). \end{aligned} \quad (19)$$

For a general quantizer, one has

$$\lambda_n = \frac{2}{\sigma^2} \sum_{l=0}^{|\mathcal{D}|-1} \frac{[\phi(\frac{t_{l+1}-\Re\{z_n\}}{\sigma/\sqrt{2}}) - \phi(\frac{t_l-\Re\{z_n\}}{\sigma/\sqrt{2}})]^2}{\Phi(\frac{t_{l+1}-\Re\{z_n\}}{\sigma/\sqrt{2}}) - \Phi(\frac{t_l-\Re\{z_n\}}{\sigma/\sqrt{2}})}, \quad (20)$$

and

$$\chi_n = \frac{2}{\sigma^2} \sum_{l=0}^{|\mathcal{D}|-1} \frac{[\phi(\frac{t_{l+1}-\Im\{z_n\}}{\sigma/\sqrt{2}}) - \phi(\frac{t_l-\Im\{z_n\}}{\sigma/\sqrt{2}})]^2}{\Phi(\frac{t_{l+1}-\Im\{z_n\}}{\sigma/\sqrt{2}}) - \Phi(\frac{t_l-\Im\{z_n\}}{\sigma/\sqrt{2}})}, \quad (21)$$

For the unquantized system, the FIM is

$$\begin{aligned} \mathbf{F}_{\text{unq}}(\boldsymbol{\kappa}) = & \frac{2}{\sigma^2} \sum_{n=1}^N \left(\frac{\partial \Re\{z_n\}}{\partial \boldsymbol{\kappa}} \left(\frac{\partial \Re\{z_n\}}{\partial \boldsymbol{\kappa}} \right)^{\text{T}} \right. \\ & \left. + \frac{\partial \Im\{z_n\}}{\partial \boldsymbol{\kappa}} \left(\frac{\partial \Im\{z_n\}}{\partial \boldsymbol{\kappa}} \right)^{\text{T}} \right). \end{aligned} \quad (22)$$

According to Theorem 1, we need to calculate $\frac{\partial \Re\{z_n\}}{\partial \boldsymbol{\kappa}}$ and $\frac{\partial \Im\{z_n\}}{\partial \boldsymbol{\kappa}}$. Since

$$z_n = \sum_{k=1}^K \tilde{g}_k e^{j((n-1)\tilde{\theta}_k + \tilde{\phi}_k)}, \quad (23)$$

we have, for $k = 1, \dots, K$,

$$\begin{aligned} \frac{\partial \Re\{z_n\}}{\partial \tilde{\theta}_k} &= -(n-1)\tilde{g}_k \sin((n-1)\tilde{\theta}_k + \tilde{\phi}_k), \\ \frac{\partial \Re\{z_n\}}{\partial \tilde{g}_k} &= \cos((n-1)\tilde{\theta}_k + \tilde{\phi}_k), \\ \frac{\partial \Re\{z_n\}}{\partial \tilde{\phi}_k} &= -\tilde{g}_k \sin((n-1)\tilde{\theta}_k + \tilde{\phi}_k), \\ \frac{\partial \Im\{z_n\}}{\partial \tilde{\theta}_k} &= (n-1)\tilde{g}_k \cos((n-1)\tilde{\theta}_k + \tilde{\phi}_k), \\ \frac{\partial \Im\{z_n\}}{\partial \tilde{g}_k} &= \sin((n-1)\tilde{\theta}_k + \tilde{\phi}_k), \\ \frac{\partial \Im\{z_n\}}{\partial \tilde{\phi}_k} &= \tilde{g}_k \cos((n-1)\tilde{\theta}_k + \tilde{\phi}_k). \end{aligned}$$

The CRB for the quantized and unquantized settings are $\text{CRB}(\boldsymbol{\kappa}) = \mathbf{F}^{-1}(\boldsymbol{\kappa})$ and $\text{CRB}_{\text{unq}}(\boldsymbol{\kappa}) = \mathbf{F}_{\text{unq}}^{-1}(\boldsymbol{\kappa})$, respectively. The CRB of the frequencies are $[\text{CRB}(\boldsymbol{\kappa})]_{1:K,1:K}$, which will be used as the performance metrics.

IV. VALSE UNDER KNOWN HETEROSCEDASTIC NOISE

As shown in [41], according to EP, the quantized (or nonlinear) measurement model can be iteratively approximated as a sequence of pseudo linear measurement model, so that linear inference algorithms could be applied. Since diagonal EP performs better than scalar EP⁵, the noise in the pseudo linear measurement model is modeled as heteroscedastic (independent components having different known variances), as opposed to [20] where the noise is homogenous. As a result, a variant of VALSE is rederived in this Section, and VALSE-EP is then developed for the nonlinear measurement model in Section V.

The pseudo linear measurement model is described as

$$\tilde{\mathbf{y}} = \mathbf{A}(\boldsymbol{\theta})\mathbf{w} + \tilde{\boldsymbol{\epsilon}}, \quad (24)$$

where $\tilde{\boldsymbol{\epsilon}} \sim \mathcal{CN}(\tilde{\boldsymbol{\epsilon}}; \mathbf{0}, \text{diag}(\tilde{\boldsymbol{\sigma}}^2))$ and $\tilde{\boldsymbol{\sigma}}^2$ is known.

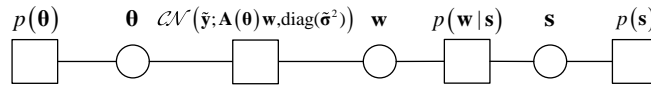


Fig. 1. The factor graph of (24) borrowed from [20].

For model (24), the factor graph is presented in Fig. 1. Given the pseudo measurements $\tilde{\mathbf{y}}$ and nuisance parameters $\boldsymbol{\beta}_w$, the above joint PDF is

$$p(\tilde{\mathbf{y}}, \boldsymbol{\Omega}; \boldsymbol{\beta}_w) \propto \left(\prod_{i=1}^N p(\theta_i) p(s_i) p(w_i | s_i) \right) p(\tilde{\mathbf{y}} | \boldsymbol{\theta}, \mathbf{w}), \quad (25)$$

where $p(\tilde{\mathbf{y}} | \boldsymbol{\theta}, \mathbf{w}) = \mathcal{CN}(\tilde{\mathbf{y}}; \mathbf{A}(\boldsymbol{\theta})\mathbf{w}, \boldsymbol{\Sigma})$, and $\boldsymbol{\Sigma} = \text{diag}(\tilde{\boldsymbol{\sigma}}^2)$. Performing the type II maximum likelihood (ML) estimation of the model parameters $\hat{\boldsymbol{\beta}}_w$ are still intractable. Thus variational approach where a given structured PDF $q(\boldsymbol{\Omega} | \tilde{\mathbf{y}})$ is used to approximate $p(\boldsymbol{\Omega} | \tilde{\mathbf{y}})$ is adopted, where $p(\boldsymbol{\Omega} | \tilde{\mathbf{y}}) = p(\tilde{\mathbf{y}}, \boldsymbol{\Omega}; \boldsymbol{\beta}_w) / p(\tilde{\mathbf{y}}; \boldsymbol{\beta}_w)$ and $p(\tilde{\mathbf{y}}; \boldsymbol{\beta}_w) = \int p(\tilde{\mathbf{y}}, \boldsymbol{\Omega}; \boldsymbol{\beta}_w) d\boldsymbol{\Omega}$. The variational Bayesian uses the Kullback-Leibler (KL) divergence of $p(\boldsymbol{\Omega} | \tilde{\mathbf{y}})$ from $q(\boldsymbol{\Omega} | \tilde{\mathbf{y}})$ to describe their dissimilarity, which is defined as [53, p. 732]

$$\text{KL}(q(\boldsymbol{\Omega} | \tilde{\mathbf{y}}) || p(\boldsymbol{\Omega} | \tilde{\mathbf{y}})) = \int q(\boldsymbol{\Omega} | \tilde{\mathbf{y}}) \log \frac{q(\boldsymbol{\Omega} | \tilde{\mathbf{y}})}{p(\boldsymbol{\Omega} | \tilde{\mathbf{y}})} d\boldsymbol{\Omega}. \quad (26)$$

⁵The code that we have made available also provides the scalar EP.

In general, the posterior PDF $q(\boldsymbol{\Omega}|\tilde{\mathbf{y}})$ is chosen from a distribution set to minimize the KL divergence. The log model evidence $\ln p(\tilde{\mathbf{y}}; \boldsymbol{\beta}_w)$ for any assumed PDF $q(\boldsymbol{\Omega}|\tilde{\mathbf{y}})$ is [53, pp. 732-733]

$$\ln p(\tilde{\mathbf{y}}; \boldsymbol{\beta}_w) = \text{KL}(q(\boldsymbol{\Omega}|\tilde{\mathbf{y}})||p(\boldsymbol{\Omega}|\tilde{\mathbf{y}})) + \mathcal{L}(q(\boldsymbol{\Omega}|\tilde{\mathbf{y}})), \quad (27)$$

where

$$\mathcal{L}(q(\boldsymbol{\Omega}|\tilde{\mathbf{y}})) = \mathbb{E}_{q(\boldsymbol{\Omega}|\tilde{\mathbf{y}})} \left[\ln \frac{p(\mathbf{y}; \boldsymbol{\Omega}; \boldsymbol{\beta}_w)}{q(\boldsymbol{\Omega}|\tilde{\mathbf{y}})} \right]. \quad (28)$$

For a given data $\tilde{\mathbf{y}}$, $\ln p(\tilde{\mathbf{y}}; \boldsymbol{\beta}_w)$ is constant, thus minimizing the KL divergence is equivalent to maximizing $\mathcal{L}(q(\boldsymbol{\Omega}|\tilde{\mathbf{y}}))$ in (27). Therefore we maximize $\mathcal{L}(q(\boldsymbol{\Omega}|\tilde{\mathbf{y}}))$ in the sequel.

For the factored PDF $q(\boldsymbol{\Omega}|\tilde{\mathbf{y}})$, the following assumptions are made:

- Given $\tilde{\mathbf{y}}$, the frequencies $\{\theta_i\}_{i=1}^N$ are mutually independent.
- The posterior of the binary hidden variables $q(\mathbf{s}|\tilde{\mathbf{y}})$ has all its mass at $\hat{\mathbf{s}}$, i.e., $q(\mathbf{s}|\tilde{\mathbf{y}}) = \delta(\mathbf{s} - \hat{\mathbf{s}})$.
- Given $\tilde{\mathbf{y}}$ and \mathbf{s} , the frequencies and weights are independent.

As a result, $q(\boldsymbol{\Omega}|\tilde{\mathbf{y}})$ can be factored as

$$q(\boldsymbol{\Omega}|\tilde{\mathbf{y}}) = \prod_{i=1}^N q(\theta_i|\tilde{\mathbf{y}})q(\mathbf{w}|\tilde{\mathbf{y}}, \mathbf{s})\delta(\mathbf{s} - \hat{\mathbf{s}}). \quad (29)$$

Due to the factorization property of (29), the frequency θ can be estimated from $q(\boldsymbol{\Omega}|\tilde{\mathbf{y}})$ as [20]

$$\hat{\theta}_i = \arg(\mathbb{E}_{q(\theta_i|\tilde{\mathbf{y}})}[e^{j\theta_i}]), \quad (30a)$$

$$\hat{\mathbf{a}}_i = \mathbb{E}_{q(\theta_i|\tilde{\mathbf{y}})}[\mathbf{a}_N(\theta_i)], \quad i \in \{1, \dots, N\}, \quad (30b)$$

where $\arg(\cdot)$ returns the angle. For the given posterior PDF $q(\mathbf{w}|\mathbf{y}, \hat{\mathbf{s}})$, the mean and covariance estimates of the weights are calculated as

$$\hat{\mathbf{w}} = \mathbb{E}_{q(\mathbf{w}|\tilde{\mathbf{y}})}[w], \quad (31a)$$

$$\hat{C}_{i,j} = \mathbb{E}_{q(\mathbf{w}|\tilde{\mathbf{y}})}[w_i w_j^*] - \hat{w}_i \hat{w}_j^*, \quad i, j \in \{1, \dots, N\}. \quad (31b)$$

Given that $q(\mathbf{s}|\tilde{\mathbf{y}}) = \delta(\mathbf{s} - \hat{\mathbf{s}})$, the posterior PDF of \mathbf{w} is

$$q(\mathbf{w}|\tilde{\mathbf{y}}) = \int q(\mathbf{w}|\tilde{\mathbf{y}}, \mathbf{s})\delta(\mathbf{s} - \hat{\mathbf{s}})d\mathbf{s} = q(\mathbf{w}|\tilde{\mathbf{y}}, \hat{\mathbf{s}}). \quad (32)$$

Let \mathcal{S} be the set of indices of the non-zero components of \mathbf{s} , i.e.,

$$\mathcal{S} = \{i | 1 \leq i \leq N, s_i = 1\}.$$

Analogously, we define $\hat{\mathcal{S}}$ based on $\hat{\mathbf{s}}$. The model order is the cardinality of $\hat{\mathcal{S}}$, i.e.,

$$\hat{K} = |\hat{\mathcal{S}}|.$$

Finally, the line spectral $\mathbf{z} = \sum_{k=1}^K \mathbf{a}(\tilde{\theta}_k) \tilde{w}_k$ is reconstructed as

$$\hat{\mathbf{z}} = \sum_{i \in \hat{\mathcal{S}}} \hat{\mathbf{a}}_i \hat{w}_i.$$

The following procedure is similar to [21]. Maximizing $\mathcal{L}(q(\mathbf{\Omega}|\tilde{\mathbf{y}}))$ with respect to all the factors is also intractable. Similar to the Gauss-Seidel method [54], \mathcal{L} is optimized over each factor $q(\theta_i|\tilde{\mathbf{y}})$, $i = 1, \dots, N$ and $q(\mathbf{w}, \mathbf{s}|\tilde{\mathbf{y}})$ separately with the others being fixed. Maximizing $\mathcal{L}(q(\mathbf{\Omega}|\tilde{\mathbf{y}}); \boldsymbol{\beta}_w)$ (28) with respect to the posterior approximation $q(\mathbf{\Omega}_d|\tilde{\mathbf{y}})$ of each latent variable $\mathbf{\Omega}_d$, $d = 1, \dots, N + 1$ yields [53, pp. 735, eq. (21.25)]

$$\ln q(\mathbf{\Omega}_d|\tilde{\mathbf{y}}) = \mathbb{E}_{q(\mathbf{\Omega} \setminus \mathbf{\Omega}_d|\tilde{\mathbf{y}})} [\ln p(\tilde{\mathbf{y}}, \mathbf{\Omega})] + \text{const}, \quad (33)$$

where the expectation is taken with respect to all the variables $\mathbf{\Omega}$ except $\mathbf{\Omega}_d$ and the constant ensures normalization of the PDF. In the ensuing three Subsections, we detail the procedures.

A. Inferring the Frequencies

For each $i = 1, \dots, N$, we maximize \mathcal{L} with respect to the factor $q(\theta_i|\tilde{\mathbf{y}})$. For $i \notin \mathcal{S}$, we have $q(\theta_i|\tilde{\mathbf{y}}) = p(\theta_i)$. For $i \in \mathcal{S}$, according to (33), the optimal factor $q(\theta_i|\tilde{\mathbf{y}})$ can be calculated as

$$\ln q(\theta_i|\tilde{\mathbf{y}}) = \mathbb{E}_{q(\mathbf{\Omega} \setminus \theta_i|\tilde{\mathbf{y}})} [\ln p(\tilde{\mathbf{y}}, \mathbf{\Omega}; \boldsymbol{\beta}_w)] + \text{const}, \quad (34)$$

Substituting (30) and (31) in (34), one obtains

$$\begin{aligned} \ln q(\theta_i|\tilde{\mathbf{y}}) &= \mathbb{E}_{q(\mathbf{\Omega} \setminus \theta_i|\tilde{\mathbf{y}})} [\ln p(\tilde{\mathbf{y}}, \mathbf{\Omega}; \boldsymbol{\beta}_w)] + \text{const} \\ &= \mathbb{E}_{q(\mathbf{z} \setminus \theta_i|\tilde{\mathbf{y}})} [\ln(p(\boldsymbol{\theta})p(\mathbf{s})p(\mathbf{w}|\mathbf{s})p(\tilde{\mathbf{y}}|\boldsymbol{\theta}, \mathbf{w}))] + \text{const} \\ &= \ln p(\theta_i) - \mathbb{E}_{q(\mathbf{z} \setminus \theta_i|\tilde{\mathbf{y}})} [(\tilde{\mathbf{y}} - \mathbf{A}_{\hat{\mathcal{S}}} \mathbf{w}_{\hat{\mathcal{S}}})^H \boldsymbol{\Sigma}^{-1} (\tilde{\mathbf{y}} - \mathbf{A}_{\hat{\mathcal{S}}} \mathbf{w}_{\hat{\mathcal{S}}})] + \text{const} \\ &= \ln p(\theta_i) + \Re\{\boldsymbol{\eta}_i^H \mathbf{a}(\theta_i)\} + \text{const}, \end{aligned} \quad (35)$$

where the complex vector $\boldsymbol{\eta}_i$ is given by

$$\boldsymbol{\eta}_i = 2\boldsymbol{\Sigma}^{-1} \left[\left(\tilde{\mathbf{y}} - \sum_{l \in \hat{\mathcal{S}} \setminus \{i\}} \hat{\mathbf{a}}_l \hat{w}_l \right) \hat{w}_i^* - \sum_{l \in \hat{\mathcal{S}} \setminus \{i\}} \hat{\mathbf{a}}_l \hat{C}_{l,i} \right], \quad (36)$$

where “ $\sim i$ ” denote the indices $\hat{\mathcal{S}}$ excluding i , $\mathbf{w}_{\hat{\mathcal{S}}}$ denotes the subvector of \mathbf{w} by choosing the $\hat{\mathcal{S}}$ rows of \mathbf{w} . The result is consistent with [20, eq. (17)] when the diagonal covariance matrix $\boldsymbol{\Sigma}$ reduces to the scaled identity matrix. $q(\theta_i|\tilde{\mathbf{y}})$ is calculated to be

$$q(\theta_i|\tilde{\mathbf{y}}) \propto p(\theta_i) \exp(\Re\{\boldsymbol{\eta}_i^H \mathbf{a}(\theta_i)\}). \quad (37)$$

Since it is hard to obtain the analytical results (30b) for the PDF (37), $q(\theta_i|\tilde{\mathbf{y}})$ is approximated as a von Mises distribution. For further details, please refer to [20, Algorithm 2: Heuristic 2].

B. Inferring the Weights and Support

Next we keep $q(\theta_i|\tilde{\mathbf{y}}), i = 1, \dots, N$ fixed and maximize \mathcal{L} w.r.t. $q(\mathbf{w}, \mathbf{s}|\tilde{\mathbf{y}})$. Define the matrices \mathbf{J} and \mathbf{h} as

$$J_{ij} = \begin{cases} \text{tr}(\boldsymbol{\Sigma}^{-1}), & i = j \\ \hat{\mathbf{a}}_i^H \boldsymbol{\Sigma}^{-1} \hat{\mathbf{a}}_j, & i \neq j \end{cases}, \quad i, j \in \{1, 2, \dots, N\}, \quad (38a)$$

$$\mathbf{h} = \hat{\mathbf{A}}^H \boldsymbol{\Sigma}^{-1} \tilde{\mathbf{y}}, \quad (38b)$$

where $\hat{\mathbf{A}} = [\hat{\mathbf{a}}_1, \dots, \hat{\mathbf{a}}_N]$. According to (33), $q(\mathbf{w}, \mathbf{s}|\tilde{\mathbf{y}})$ can be calculated as

$$\begin{aligned} \ln q(\mathbf{w}, \mathbf{s}|\tilde{\mathbf{y}}) &= \mathbb{E}_{q(\boldsymbol{\Omega}|\tilde{\mathbf{y}})} [\ln p(\tilde{\mathbf{y}}, \boldsymbol{\Omega}; \boldsymbol{\beta}_w)] + \text{const} \\ &= \mathbb{E}_{q(\boldsymbol{\theta}|\tilde{\mathbf{y}})} \left[\sum_{i=1}^N \ln p(s_i) + \ln p(\mathbf{w}|\mathbf{s}) + \ln p(\tilde{\mathbf{y}}|\boldsymbol{\theta}, \mathbf{w}) \right] + \text{const} \\ &= -(\mathbf{w}_S - \hat{\mathbf{w}}_S)^H \hat{\mathbf{C}}_S^{-1} (\mathbf{w}_S - \hat{\mathbf{w}}_S) + \text{const}, \end{aligned} \quad (39)$$

where

$$\hat{\mathbf{C}}_S = \left(\mathbf{J}_S + \frac{\mathbf{I}_{|S|}}{\tau} \right)^{-1}, \quad (40a)$$

$$\hat{\mathbf{w}}_S = \hat{\mathbf{C}}_S \mathbf{h}_S. \quad (40b)$$

It is worth noting that calculating $\hat{\mathbf{C}}_S$ and $\hat{\mathbf{w}}_S$ involves a matrix inversion. In the Appendix X-A, it is shown that $\hat{\mathbf{C}}_S$ and $\hat{\mathbf{w}}_S$ can be updated efficiently.

From (29), the posterior approximation $q(\mathbf{w}, \mathbf{s}|\tilde{\mathbf{y}})$ can be factored as the product of $q(\mathbf{w}|\tilde{\mathbf{y}}, \mathbf{s})$ and $\delta(\mathbf{s} - \hat{\mathbf{s}})$. According to the formulation of (39), for a given $\hat{\mathbf{s}}$, $q(\mathbf{w}_{\hat{S}}|\tilde{\mathbf{y}})$ is a complex Gaussian distribution, and $q(\mathbf{w}|\tilde{\mathbf{y}}; \hat{\mathbf{s}})$ is

$$q(\mathbf{w}|\tilde{\mathbf{y}}; \hat{\mathbf{s}}) = \mathcal{CN}(\mathbf{w}_{\hat{S}}; \hat{\mathbf{w}}_{\hat{S}}, \hat{\mathbf{C}}_{\hat{S}}) \prod_{i \notin \hat{S}} \delta(w_i). \quad (41)$$

Plugging the postulated PDF (29) in (28), one has

$$\begin{aligned} \mathcal{L}(q(\boldsymbol{\Omega}|\tilde{\mathbf{y}}); \hat{\mathbf{s}}) &= \mathbb{E}_{q(\boldsymbol{\Omega}|\tilde{\mathbf{y}})} \left[\frac{p(\tilde{\mathbf{y}}, \boldsymbol{\Omega}; \hat{\mathbf{s}})}{q(\boldsymbol{\Omega}|\tilde{\mathbf{y}})} \right] \\ &= \mathbb{E}_{q(\boldsymbol{\Omega}|\tilde{\mathbf{y}})} \left[\sum_{i=1}^N \ln p(s_i) + \ln p(\mathbf{w}|\mathbf{s}) + \ln p(\tilde{\mathbf{y}}|\boldsymbol{\theta}, \mathbf{w}) - \ln q(\mathbf{w}|\tilde{\mathbf{y}}) \right] + \text{const} \\ &= -\ln \det(\mathbf{J}_{\hat{S}} + \frac{1}{\tau} \mathbf{I}_{|\hat{S}|}) + \mathbf{h}_{\hat{S}}^H (\mathbf{J}_{\hat{S}} + \frac{1}{\tau} \mathbf{I}_{|\hat{S}|})^{-1} \mathbf{h}_{\hat{S}} + \|\hat{\mathbf{s}}\|_0 \ln \frac{\rho}{1-\rho} + \|\hat{\mathbf{s}}\|_0 \ln \frac{1}{\tau} + \text{const} \\ &\triangleq \ln Z(\mathbf{s})|_{\mathbf{s}=\hat{\mathbf{s}}} \end{aligned} \quad (42)$$

Then we need to find $\hat{\mathbf{s}}$ which maximizes $\ln Z(\mathbf{s})$, i.e.,

$$\hat{\mathbf{s}} = \underset{\mathbf{s}}{\operatorname{argmax}} \ln Z(\mathbf{s}). \quad (43)$$

The computation cost of enumerative method to find the globally optimal binary sequence \mathbf{s} of (43) is $O(2^N)$, which is impractical for typical values of N . In Appendix X-A, a greedy iterative search strategy similar to [20] is proposed. Since each step increases the objective function (which is bounded) and \mathbf{s} can take a finite number of values (at most 2^N), the method converges in a finite number of steps to some local optimum. In general, numerical experiments show that $O(\hat{K})$ steps is often enough to find the local optimum.

Once \mathbf{s} is updated as \mathbf{s}' , the mean $\hat{\mathbf{w}}'_{\mathcal{S}}$, and covariance $\hat{\mathbf{C}}'_{\mathcal{S}}$, of the weights should be updated accordingly. For the active case, $\hat{\mathbf{w}}'_{\mathcal{S}}$ and covariance $\hat{\mathbf{C}}'_{\mathcal{S}}$ are updated according to (85) and (84), while for the deactive case, $\hat{\mathbf{w}}'_{\mathcal{S}}$ and covariance $\hat{\mathbf{C}}'_{\mathcal{S}}$ are updated according to (91) and (90).

C. Estimating the Model Parameters

After updating the frequencies and weights, the model parameters $\beta_w = \{\rho, \tau\}$ are estimated via maximizing the lower bound $\mathcal{L}(q(\boldsymbol{\Omega}|\tilde{\mathbf{y}}); \beta_w)$ for fixed $q(\boldsymbol{\Omega}|\tilde{\mathbf{y}})$. Straightforward calculation shows that

$$\begin{aligned} \mathcal{L}(q(\boldsymbol{\Omega}|\tilde{\mathbf{y}}); \beta_w) &= \mathbb{E}_{q(\boldsymbol{\Omega}|\tilde{\mathbf{y}})} \left[\ln \frac{p(\tilde{\mathbf{y}}, \boldsymbol{\Omega}; \beta_w)}{q(\boldsymbol{\Omega}|\tilde{\mathbf{y}})} \right] \\ &= \mathbb{E}_{q(\boldsymbol{\Omega}|\tilde{\mathbf{y}})} \left[\sum_{i=1}^N \ln p(s_i) + \ln p(\mathbf{w}|\mathbf{s}) \right] + \text{const} \\ &= \|\hat{\mathbf{s}}\|_0 \ln \rho + (N - \|\hat{\mathbf{s}}\|_0) \ln(1 - \rho) + \|\hat{\mathbf{s}}\|_0 \ln \frac{1}{\pi\tau} - \mathbb{E}_{q(\mathbf{w}|\tilde{\mathbf{y}})} \left[\frac{1}{\tau} \mathbf{w}_{\hat{\mathcal{S}}}^H \mathbf{w}_{\hat{\mathcal{S}}} \right] + \text{const}. \end{aligned} \quad (44)$$

Because

$$\mathbb{E}_{q(\mathbf{w}|\tilde{\mathbf{y}})} [\mathbf{w}_{\hat{\mathcal{S}}}^H \mathbf{w}_{\hat{\mathcal{S}}}] = \mathbb{E}_{q(\mathbf{w}|\tilde{\mathbf{y}})} \left[\sum_{i \in \hat{\mathcal{S}}} w_i^* w_i \right] = \hat{\mathbf{w}}_{\hat{\mathcal{S}}}^H \hat{\mathbf{w}}_{\hat{\mathcal{S}}} + \text{tr}(\hat{\mathbf{C}}_{\hat{\mathcal{S}}}),$$

we obtain

$$\mathcal{L}(q(\boldsymbol{\Omega}|\tilde{\mathbf{y}}); \beta_w) = -\frac{1}{\tau} [(\hat{\mathbf{w}}_{\hat{\mathcal{S}}}^H \hat{\mathbf{w}}_{\hat{\mathcal{S}}}) + \text{tr}(\hat{\mathbf{C}}_{\hat{\mathcal{S}}})] + \|\hat{\mathbf{s}}\|_0 \left(\ln \frac{\rho}{1 - \rho} - \ln \tau \right) + N \ln(1 - \rho) + \text{const}.$$

Setting $\frac{\partial \mathcal{L}}{\partial \rho} = 0$, $\frac{\partial \mathcal{L}}{\partial \tau} = 0$, we have

$$\begin{aligned} \hat{\rho} &= \frac{\|\hat{\mathbf{s}}\|_0}{N}, \\ \hat{\tau} &= \frac{\hat{\mathbf{w}}_{\hat{\mathcal{S}}}^H \hat{\mathbf{w}}_{\hat{\mathcal{S}}} + \text{tr}(\hat{\mathbf{C}}_{\hat{\mathcal{S}}})}{\|\hat{\mathbf{s}}\|_0}. \end{aligned} \quad (45)$$

V. VALSE-EP ALGORITHM

In this section, the VALSE-EP algorithm is developed based on EP [40]. According to EP and the factor graph presented in Fig. 2, the quantization model is iteratively reduced to a sequence of pseudo unquantized models [41]. As a result, the original quantized LSE problem is decoupled into two modules: the VALSE module named module A and the componentwise MMSE module named module B. The two modules iteratively exchange the extrinsic information and refine their estimates.

Note that the factor graph shown in Fig. 2 only requires that $p(\mathbf{y}|\mathbf{z}) = \prod_{n=1}^N p(y_n|z_n)$. As a result, it is believed that VALSE-EP is very general and can have a wider implication to a range of nonlinear identification issues in signal processing, such as phase retrieval $\mathbf{y} = |\mathbf{z} + \epsilon|$ in noncoherent channel estimation [55], impulsive noise scenario $\mathbf{y} = \mathbf{z} + \epsilon$ where ϵ is the impulsive noise.

The detailed VALSE-EP is presented as follows.

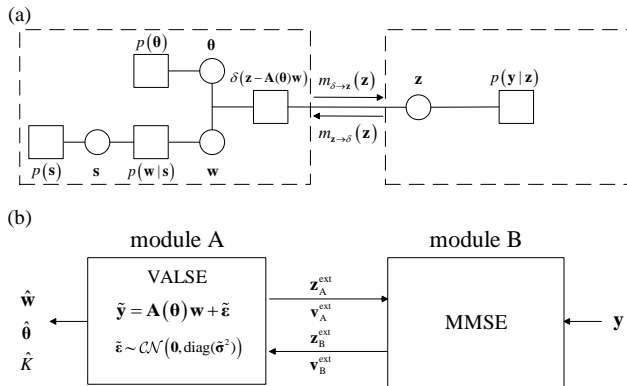


Fig. 2. Factor graph of the joint PDF (10) and the module of the VALSE-EP algorithm. Here the circle denotes the variable node, and the square denotes the factor node. According to the dashed block diagram in Fig. 1 (a), the problem can be decomposed as two modules in Fig. 1 (b), where module A corresponds to the standard linear model, and module B corresponds to the componentwise MMSE estimation. Intuitively, the problem can be solved by iterating between the two modules, where module A performs a variant of VALSE algorithm, and module B performs the componentwise MMSE estimation.

A. Componentwise MMSE module

The factor graph and the algorithm module are shown in Fig. 2. Specifically, in the t th iteration, let $m_{\delta \rightarrow \mathbf{z}}^t(\mathbf{z}) = \mathcal{CN}(\mathbf{z}_A^{\text{ext}}(t), \text{diag}(\mathbf{v}_A^{\text{ext}}(t)))$ denote the message transmitted from the factor node $\delta(\mathbf{z} - \mathbf{A}\mathbf{w})$ to the variable node \mathbf{z} , which can be regarded as an extrinsic information from module A. According to

EP, the message $m_{\mathbf{z} \rightarrow \delta}^t(\mathbf{z})$ transmitted from the variable node \mathbf{z} to the factor node $\delta(\mathbf{z} - \mathbf{A}\mathbf{w})$ can be calculated as [40]

$$m_{\mathbf{z} \rightarrow \delta}^t(\mathbf{z}) \propto \frac{\text{Proj}[m_{\delta \rightarrow \mathbf{z}}^t(\mathbf{z})p(\mathbf{y}|\mathbf{z})]}{m_{\delta \rightarrow \mathbf{z}}^t(\mathbf{z})} \triangleq \frac{\text{Proj}[q_{\mathbf{B}}^t(\mathbf{z})]}{m_{\delta \rightarrow \mathbf{z}}^t(\mathbf{z})}, \quad (46)$$

where $p(\mathbf{y}|\mathbf{z}) = \prod_{n=1}^N p(y_n|z_n)$ and $p(y_n|z_n)$ is (17), \propto denotes identity up to a normalizing constant.

First, the posterior means and variances of \mathbf{z} in module B can be obtained, i.e.,

$$\mathbf{z}_{\mathbf{B}}^{\text{post}}(t) = \text{E}[\mathbf{z}|q_{\mathbf{B}}^t(\mathbf{z})], \quad (47)$$

$$\mathbf{v}_{\mathbf{B}}^{\text{post}}(t) = \text{Var}[\mathbf{z}|q_{\mathbf{B}}^t(\mathbf{z})], \quad (48)$$

where $\text{E}[\cdot|q_{\mathbf{B}}^t(\mathbf{z})]$ and $\text{Var}[\cdot|q_{\mathbf{B}}^t(\mathbf{z})]$ are the mean and variance operations taken componentwise with respect to the distribution $\propto q_{\mathbf{B}}^t(\mathbf{z})$ and closed-form expression exists for quantized measurements [42].

As a result, $\text{Proj}[q_{\mathbf{B}}^t(\mathbf{z})]$ is

$$\text{Proj}[q_{\mathbf{B}}^t(\mathbf{z})] = \mathcal{CN}(\mathbf{z}; \mathbf{z}_{\mathbf{B}}^{\text{post}}(t), \text{diag}(\mathbf{v}_{\mathbf{B}}^{\text{post}}(t))). \quad (49)$$

Substituting (49) in (46), the message $m_{\mathbf{z} \rightarrow \delta}^t(\mathbf{z})$ from the variable node \mathbf{z} to the factor node $\delta(\mathbf{z} - \mathbf{A}\mathbf{x})$ is calculated as

$$m_{\mathbf{z} \rightarrow \delta}^t(\mathbf{z}) \propto \frac{\mathcal{CN}(\mathbf{z}; \mathbf{z}_{\mathbf{B}}^{\text{post}}(t), \text{diag}(\mathbf{v}_{\mathbf{B}}^{\text{post}}(t)))}{\mathcal{CN}(\mathbf{z}; \mathbf{z}_{\mathbf{A}}^{\text{ext}}(t), \text{diag}(\mathbf{v}_{\mathbf{A}}^{\text{ext}}(t)))} \propto \mathcal{CN}(\mathbf{z}; \mathbf{z}_{\mathbf{B}}^{\text{ext}}(t), \text{diag}(\mathbf{v}_{\mathbf{B}}^{\text{ext}}(t))), \quad (50)$$

which can be viewed as the extrinsic information from module B and $\mathbf{z}_{\mathbf{B}}^{\text{ext}}(t)$ and $\mathbf{v}_{\mathbf{B}}^{\text{ext}}(t)$ are [41]

$$\mathbf{v}_{\mathbf{B}}^{\text{ext}}(t) = \left(\frac{1}{\mathbf{v}_{\mathbf{B}}^{\text{post}}(t)} - \frac{1}{\mathbf{v}_{\mathbf{A}}^{\text{ext}}(t)} \right)^{-1}, \quad (51a)$$

$$\mathbf{z}_{\mathbf{B}}^{\text{ext}}(t) = \mathbf{v}_{\mathbf{B}}^{\text{ext}}(t) \odot \left(\frac{\mathbf{z}_{\mathbf{B}}^{\text{post}}(t)}{\mathbf{v}_{\mathbf{B}}^{\text{post}}(t)} - \frac{\mathbf{z}_{\mathbf{A}}^{\text{ext}}(t)}{\mathbf{v}_{\mathbf{A}}^{\text{ext}}(t)} \right), \quad (51b)$$

where \odot denotes componentwise multiplication.

In addition, EM algorithm can be incorporated to learn the noise variance σ^2 [59]. The posterior distribution of \mathbf{z} is approximated as (49). We compute the expected complete log-likelihood function $\log p(\mathbf{y}|\mathbf{z}; \sigma^2) + \log m_{\delta \rightarrow \mathbf{z}}^t(\mathbf{z})$ with respect to $q(\mathbf{z}|\mathbf{y}; \sigma^2(t))$, and drop the irrelevant terms to have

$$Q(\sigma^2; \sigma^2(t)) = \text{E}_{q(\mathbf{z}|\mathbf{y}; \sigma^2(t))} [\log p(\mathbf{y}|\mathbf{z}; \sigma^2)]. \quad (52)$$

Then σ^2 is updated as

$$\sigma^2(t+1) = \underset{\sigma^2}{\text{argmax}} Q(\sigma^2; \sigma^2(t)). \quad (53)$$

For the AWGN model

$$\mathbf{y} = \mathbf{z} + \boldsymbol{\epsilon}, \quad (54)$$

where $\epsilon \sim \mathcal{CN}(\epsilon; \mathbf{0}, \sigma^2 \mathbf{I})$, the posterior PDF $q(\mathbf{z}|\mathbf{y}; \sigma^2(t))$ is

$$q(\mathbf{z}|\mathbf{y}; \sigma^2(t)) = \mathcal{CN}(\mathbf{z}; \mathbf{z}_B^{\text{post}}(t), \text{diag}(\mathbf{v}_B^{\text{post}}(t))). \quad (55)$$

Substituting (55), (54) and (52) in (53), the noise variance σ^2 is estimated as

$$\sigma^2(t+1) = \frac{\|\mathbf{y} - \mathbf{z}_B^{\text{post}}(t)\|^2 + \mathbf{1}^T \mathbf{v}_B^{\text{post}}(t)}{M}. \quad (56)$$

For arbitrary $p(\mathbf{y}|\mathbf{z})$ including the quantized case, we also obtain an approximate update equation. From the definition of $m_{\mathbf{z} \rightarrow \delta}(\mathbf{z})$ and $\mathbf{z} = \mathbf{A}(\boldsymbol{\theta})\mathbf{x}$, we obtain a pseudo measurement model

$$\tilde{\mathbf{y}}(t) = \mathbf{z} + \tilde{\boldsymbol{\epsilon}}(t), \quad (57)$$

where $\tilde{\mathbf{y}}(t) = \mathbf{z}_B^{\text{ext}}(t)$, $\tilde{\boldsymbol{\epsilon}}(t) \sim \mathcal{CN}(\boldsymbol{\epsilon}(t); \mathbf{0}, \text{diag}(\tilde{\boldsymbol{\sigma}}^2(t)))$ and $\tilde{\boldsymbol{\sigma}}^2(t) = \mathbf{v}_B^{\text{ext}}(t)$. The noise variance σ^2 is updated as [51]

$$\sigma^2(t+1) = \frac{\|\tilde{\mathbf{y}}(t) - \mathbf{z}_B^{\text{post}}(t)\|^2 + \mathbf{1}^T \mathbf{v}_B^{\text{post}}(t)}{M}. \quad (58)$$

Note that (56) is a special case of (58), as for the AWGN model (54), $\tilde{\mathbf{y}} = \mathbf{y}$ is proved later according to (75a) and (76a).

B. VALSE module

According to (50), the message $m_{\mathbf{z} \rightarrow \delta}^t(\mathbf{z})$ (nonGaussian likelihood) transmitted from the variable node \mathbf{z} to the factor node $\delta(\mathbf{z} - \mathbf{A}\mathbf{x})$ is iteratively approximated as a Gaussian distribution (Gaussian likelihood), and the factor graph is shown in Fig. 3 (a). Based on the definition of the factor node $\delta(\mathbf{z} - \mathbf{A}\mathbf{x})$ and the message $m_{\mathbf{z} \rightarrow \delta}^t(\mathbf{z})$ transmitted from the variable node \mathbf{z} to the factor node $\delta(\mathbf{z} - \mathbf{A}\mathbf{w})$, a pseudo linear measurement model

$$\tilde{\mathbf{y}}(t+1) = \mathbf{A}(\boldsymbol{\theta})\mathbf{w} + \tilde{\boldsymbol{\epsilon}}(t+1), \quad (59)$$

is obtained, where $\tilde{\boldsymbol{\epsilon}}(t+1) \sim \mathcal{CN}(\tilde{\boldsymbol{\epsilon}}(t+1); \mathbf{0}, \text{diag}(\tilde{\boldsymbol{\sigma}}^2(t+1)))$, and

$$\tilde{\mathbf{y}}(t+1) = \mathbf{z}_B^{\text{ext}}(t), \quad (60)$$

$$\tilde{\boldsymbol{\sigma}}^2(t+1) = \mathbf{v}_B^{\text{ext}}(t). \quad (61)$$

As a result, the pseudo factor graph Fig. 3 (b) is obtained and is equivalent to Fig. 1. In Section IV, a variant of VALSE is rederived. Here we run the VALSE in a single iteration and output the approximated posterior PDF $q(\mathbf{w}_{\hat{\delta}}|\tilde{\mathbf{y}})$ and $q(\boldsymbol{\theta}|\tilde{\mathbf{y}})$.

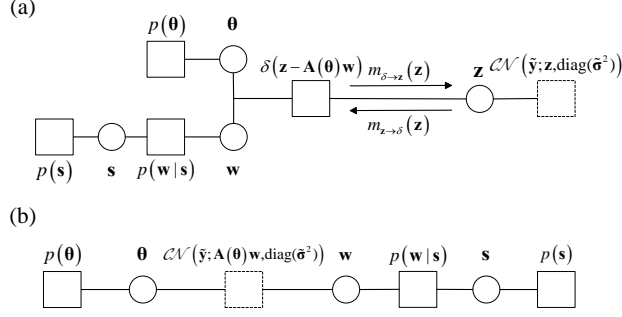


Fig. 3. Two equivalent factor graphs of the joint PDF (25). The dashed square denotes the pseudo factor node.

C. From VALSE module to MMSE module

According to the approximated posterior PDF $q(\mathbf{w}_{\hat{\mathcal{S}}}|\tilde{\mathbf{y}})$ and $q(\theta|\tilde{\mathbf{y}})$, we calculate the message $m_{\delta \rightarrow \mathbf{z}}^{t+1}(\mathbf{z})$ as

$$m_{\delta \rightarrow \mathbf{z}}^{t+1}(\mathbf{z}) \propto \frac{\text{Proj}[\int q(\mathbf{w}_{\hat{\mathcal{S}}}|\tilde{\mathbf{y}})\delta(\mathbf{z} - \mathbf{A}_{\hat{\mathcal{S}}}(\theta)\mathbf{w}_{\hat{\mathcal{S}}})q(\theta|\tilde{\mathbf{y}})d\mathbf{w}_{\hat{\mathcal{S}}}d\theta]}{m_{\mathbf{z} \rightarrow \delta}^t(\mathbf{z})}$$

$$\triangleq \frac{\text{Proj}[q_A^{t+1}(\mathbf{z})]}{m_{\mathbf{z} \rightarrow \delta}^t(\mathbf{z})}. \quad (62)$$

According to (62), the posterior means and variances of \mathbf{z} averaged over $q_A^{t+1}(\mathbf{z})$ in module A are

$$\mathbf{z}_A^{\text{post}}(t+1) = \hat{\mathbf{A}}_{\hat{\mathcal{S}}}\hat{\mathbf{w}}_{\hat{\mathcal{S}}}, \quad (63)$$

$$\mathbf{v}_A^{\text{post}}(t+1) = \text{diag}(\hat{\mathbf{A}}_{\hat{\mathcal{S}}}\hat{\mathbf{C}}_{\hat{\mathcal{S}}}\hat{\mathbf{A}}_{\hat{\mathcal{S}}}^H) + \left(\hat{\mathbf{w}}_{\hat{\mathcal{S}}}^H\hat{\mathbf{w}}_{\hat{\mathcal{S}}}\mathbf{1}_N - |\hat{\mathbf{A}}_{\hat{\mathcal{S}}}|^2|\hat{\mathbf{w}}_{\hat{\mathcal{S}}}|^2\right) + \left[\text{tr}(\hat{\mathbf{C}}_{\hat{\mathcal{S}}})\mathbf{1}_N - |\hat{\mathbf{A}}_{\hat{\mathcal{S}}}|^2\text{diag}(\hat{\mathbf{C}}_{\hat{\mathcal{S}}})\right], \quad (64)$$

where details of (64) are postponed to Appendix X-B. Thus $\text{Proj}[q_A^{t+1}(\mathbf{z})]$ is

$$\text{Proj}[q_A^{t+1}(\mathbf{z})] = \mathcal{CN}(\mathbf{z}; \mathbf{z}_A^{\text{post}}(t+1), \text{diag}(\mathbf{v}_A^{\text{post}}(t+1))). \quad (65)$$

According to (62), $m_{\delta \rightarrow \mathbf{z}}^{t+1}(\mathbf{z})$ is calculated to be

$$m_{\delta \rightarrow \mathbf{z}}^{t+1}(\mathbf{z}) = \mathcal{CN}(\mathbf{z}; \mathbf{z}_A^{\text{ext}}(t+1), \text{diag}(\mathbf{v}_A^{\text{ext}}(t+1))), \quad (66)$$

where the extrinsic means $\mathbf{z}_A^{\text{ext}}(t+1)$ and variances $\mathbf{v}_A^{\text{ext}}(t+1)$ are given by [41]

$$\frac{1}{\mathbf{v}_A^{\text{ext}}(t+1)} = \frac{1}{\mathbf{v}_A^{\text{post}}(t+1)} - \frac{1}{\tilde{\sigma}_w^2(t+1)}, \quad (67)$$

$$\mathbf{z}_A^{\text{ext}}(t+1) = \mathbf{v}_A^{\text{ext}}(t+1) \odot \left(\frac{\mathbf{z}_A^{\text{post}}(t+1)}{\mathbf{v}_A^{\text{post}}(t+1)} - \frac{\tilde{\mathbf{y}}(t+1)}{\tilde{\sigma}_w^2(t+1)} \right), \quad (68)$$

and we input them to module B. The algorithm iterates until convergence or the maximum number of iterations is reached. The VALSE-EP algorithm is summarized as Algorithm 1.

Algorithm 1 VALSE-EP algorithm

- 1: Set the number of iterations T and implement the initialization in Subsection V-D.
 - 2: **for** $t = 1, \dots, T$ **do**
 - 3: Update \mathbf{J} (38a) and \mathbf{h} (38b) using $\tilde{\mathbf{y}}(t)$ and $\tilde{\boldsymbol{\sigma}}^2(t)$.
 - 4: Update $\hat{\mathbf{s}}, \hat{\mathbf{w}}_{\hat{\mathbf{s}}}$ and $\hat{\mathbf{C}}_{\hat{\mathbf{s}}}$ (Section IV-B).
 - 5: Update $\hat{\rho}, \hat{\tau}$ (45) (Section IV-C).
 - 6: Update $\boldsymbol{\eta}_i$ and $\hat{\mathbf{a}}_i$ for all $i \in \hat{\mathcal{S}}$ (Section IV-A).
 - 7: Calculate the posterior means $\mathbf{z}_{\mathbf{A}}^{\text{post}}(t)$ (63) and variances $\mathbf{v}_{\mathbf{A}}^{\text{post}}(t)$ (64).
 - 8: Compute the extrinsic mean and variance of \mathbf{z} as $\mathbf{v}_{\mathbf{A}}^{\text{ext}}(t)$ (67), $\mathbf{z}_{\mathbf{A}}^{\text{ext}}(t)$ (68).
 - 9: Compute the post mean and variance of \mathbf{z} as $\mathbf{z}_{\mathbf{B}}^{\text{post}}(t)$ (47), $\mathbf{v}_{\mathbf{B}}^{\text{post}}(t)$ (48).
 - 10: Compute the extrinsic mean and variance of \mathbf{z} as $\mathbf{z}_{\mathbf{B}}^{\text{ext}}(t)$ (51b) and $\mathbf{v}_{\mathbf{B}}^{\text{ext}}(t)$ (51a), and set $\tilde{\boldsymbol{\sigma}}^2(t+1) = \mathbf{v}_{\mathbf{B}}^{\text{ext}}(t)$ and $\tilde{\mathbf{y}}(t+1) = \mathbf{z}_{\mathbf{B}}^{\text{ext}}(t)$. Implement EM to estimate the noise variance as $\sigma^2(t+1)$ (58).
 - 11: **end for**
 - 12: Return $\hat{\boldsymbol{\theta}}, \hat{\mathbf{w}}, \hat{\mathbf{z}}$ and \hat{K} .
-

D. Initialization

The initialization of VALSE-EP is presented. First, the additive quantization noise model (AQNM) [56]

$$\mathbf{y}_q = \mathbf{z} + \boldsymbol{\epsilon} + \boldsymbol{\epsilon}_q, \quad (69)$$

is adopted, where the output levels \mathbf{y}_q are the midpoints of the quantization interval, $\boldsymbol{\epsilon}_q$ is the quantization error. First, the noise variance σ^2 is initialized. For $n' = 1, \dots, N-1$, we calculate $\gamma_{n'} = \frac{1}{N} \sum_{(k', l') \in \Upsilon_{n'}} y_{k'} y_{l'}^*$ with $\Upsilon_{n'} = \{(k', l') | 1 \leq k', l' \leq N-1, k' - l' = n'\}$. We use γ to build a Toeplitz estimate of $E[\mathbf{y}_q \mathbf{y}_q^H]$. Then, we initialize σ^2 with the average of the lower quarter of the eigenvalues of the Toeplitz matrix (ignoring the quantization noise). Typically, it is found that setting $\mathbf{v}_{\mathbf{A}}^{\text{ext}}$ ranging from $1 \sim 10^2$ works well. Here we initialize $\mathbf{z}_{\mathbf{A}}^{\text{ext}} = \mathbf{0}$ and $\mathbf{v}_{\mathbf{A}}^{\text{ext}} = \mathbf{10}$. After performing the MMSE estimation in module B, $\tilde{\mathbf{y}} = \mathbf{z}_{\mathbf{B}}^{\text{ext}}$ and $\tilde{\boldsymbol{\sigma}}^2 = \mathbf{v}_{\mathbf{B}}^{\text{ext}}$ are obtained. Given that $E[\tilde{\mathbf{y}} \text{diag}(\tilde{\boldsymbol{\sigma}}^{-2}) \tilde{\mathbf{y}}^H] = N + \rho N \tau \text{tr}(\text{diag}(\tilde{\boldsymbol{\sigma}}^{-2}))$, we set $\hat{\rho} = 0.5$ and let $\hat{\tau} = (\tilde{\mathbf{y}} \text{diag}(\tilde{\boldsymbol{\sigma}}^{-2}) \tilde{\mathbf{y}}^H - N) / (\hat{\rho} N \text{tr}(\text{diag}(\tilde{\boldsymbol{\sigma}}^{-2})))$. Then in step i , when the first $i-1$ PDFs of the frequencies are initialized, the estimates $\{\hat{w}_k\}_{k=1}^{i-1}$ and the residual $\mathbf{y}_{i-1}^r = \tilde{\mathbf{y}} - \sum_{k=1}^{i-1} \hat{\mathbf{a}}_k \hat{w}_k$ are obtained. Then initialize $q(\theta_i | \mathbf{y}_{i-1}^r) \propto \exp(|\mathbf{y}_{i-1}^r \text{diag}(\tilde{\boldsymbol{\sigma}}^{-2}) \mathbf{a}(\theta)|^2 / N)$ and project it as a von Mises distribution and compute $\hat{\mathbf{a}}_i$.

E. Computation Complexity

From Algorithm 1, it can be seen that VALSE-EP involves the componentwise MMSE operation and VALSE. For the componentwise MMSE operation, the computation complexity is $O(N\hat{K})$. As for the VALSE, the complexity per iteration is dominated by the two steps: the maximization of $\ln Z(\mathbf{s})$ and the approximations of the posterior PDF $q(\theta_i|\mathbf{y})$ by mixtures of von Mises PDFs. This work approximates the posterior PDF $q(\theta_i|\mathbf{y})$ by Heuristic 2 in [20, Algorithm 2]. Thus the complexity of the two steps are $O(N\hat{K}^3)$ and $O(N^2)$ [20]. Therefore, the complexity of VALSE-EP is comparable to that of VALSE.

VI. RELATIONSHIP BETWEEN VALSE-EP AND VALSE UNDER UNQUANTIZED SETTING

Before revealing the relation between VALSE-EP and VALSE under unquantized setting, the following properties are revealed.

Property 1 *The noise variance estimate in VALSE can be equivalently derived in EM step.*

PROOF In [20], the noise variance is estimated as (reformulated as our notation)

$$\sigma_{\text{VA}}^2(t+1) = \frac{1}{N} \|\mathbf{y} - \sum_{i \in \mathcal{S}} \hat{\mathbf{a}}_i \hat{w}_i\|_2^2 + \frac{1}{N} \text{tr}(\mathbf{J}'_{\mathcal{S}} \hat{\mathbf{C}}_{\mathcal{S}}) + \sum_{i \in \mathcal{S}} |\hat{w}_i|^2 (1 - \|\hat{\mathbf{a}}_i\|_2^2 / N), \quad (70)$$

where $\mathbf{J}'_{ii} = N$ and $\mathbf{J}'_{ij} = \hat{\mathbf{a}}_i^H \hat{\mathbf{a}}_j$. According to EM, the noise variance $\sigma^2(t+1)$ in module A should be updated as (replacing $\mathbf{z}_B^{\text{post}}(t)$ and $\mathbf{v}_B^{\text{post}}(t)$ with $\mathbf{z}_A^{\text{post}}(t)$ and $\mathbf{v}_A^{\text{post}}(t)$ in (56), respectively)

$$\sigma^2(t+1) = \frac{\|\mathbf{y} - \mathbf{z}_A^{\text{post}}(t)\|^2 + \mathbf{1}^T \mathbf{v}_A^{\text{post}}(t)}{N}. \quad (71)$$

Substituting $\mathbf{z}_A^{\text{post}}(t)$ (63) and $\mathbf{v}_A^{\text{post}}(t)$ (64) in (71) and utilizing $\mathbf{J}' = \hat{\mathbf{A}}^H \hat{\mathbf{A}} + N\mathbf{I}_N - \text{diag}(\text{diag}(\hat{\mathbf{A}}^H \hat{\mathbf{A}}))$, one can show that $\sigma^2(t+1) = \sigma_{\text{VA}}^2(t+1)$. \blacksquare

Property 1 reveals that the noise variance estimates of both VALSE-EP and VALSE can be derived via the EM step. For the VALSE algorithm, the noise variance estimate of the EM step is performed in module A, while for VALSE-EP, the noise variance estimate of the EM step is performed in module B. In the following text, the relationships between the posterior means and variances of VALSE and that of VALSE-EP are derived.

Property 2 *The relationships between the posterior means $\mathbf{z}_B^{\text{post}}(t)$ and variances $\mathbf{v}_B^{\text{post}}(t)$ of \mathbf{z} in module B and the posterior means $\mathbf{z}_A^{\text{post}}(t)$ and variances $\mathbf{v}_A^{\text{post}}(t)$ of \mathbf{z} in module A are*

$$\frac{1}{\mathbf{v}_B^{\text{post}}(t+1)} = \frac{1}{\mathbf{v}_A^{\text{post}}(t+1)} - \frac{1}{\sigma^2(t)} + \frac{1}{\sigma^2(t+1)}, \quad (72a)$$

$$\frac{\mathbf{z}_B^{\text{post}}(t+1)}{\mathbf{v}_B^{\text{post}}(t+1)} = \frac{\mathbf{z}_A^{\text{post}}(t+1)}{\mathbf{v}_A^{\text{post}}(t+1)} - \mathbf{y} \left(\frac{1}{\sigma^2(t)} - \frac{1}{\sigma^2(t+1)} \right). \quad (72b)$$

PROOF For the t th iteration, let the extrinsic means and variances of \mathbf{z} from module A be $\mathbf{z}_A^{\text{ext}}(t)$ and $\mathbf{v}_A^{\text{ext}}(t)$ (Step 8 in Algorithm 1), and the noise variance be $\sigma^2(t)$. The posterior variances (48) and means (47) of \mathbf{z} are

$$\frac{1}{\mathbf{v}_B^{\text{post}}(t)} = \frac{1}{\mathbf{v}_A^{\text{ext}}(t)} + \frac{1}{\sigma^2(t)}, \quad (73a)$$

$$\frac{\mathbf{z}_B^{\text{post}}(t)}{\mathbf{v}_B^{\text{post}}(t)} = \frac{\mathbf{z}_A^{\text{ext}}(t)}{\mathbf{v}_A^{\text{ext}}(t)} + \frac{\mathbf{y}}{\sigma^2(t)}. \quad (73b)$$

Then the extrinsic means and variances of \mathbf{z} from module B $\mathbf{z}_B^{\text{ext}}(t)$ and $\mathbf{v}_B^{\text{ext}}(t)$ are

$$\frac{1}{\mathbf{v}_B^{\text{ext}}(t)} = \frac{1}{\mathbf{v}_B^{\text{post}}(t)} - \frac{1}{\mathbf{v}_A^{\text{ext}}(t)}, \quad (74a)$$

$$\frac{\mathbf{z}_B^{\text{ext}}(t)}{\mathbf{v}_B^{\text{ext}}(t)} = \frac{\mathbf{z}_B^{\text{post}}(t)}{\mathbf{v}_B^{\text{post}}(t)} - \frac{\mathbf{z}_A^{\text{ext}}(t)}{\mathbf{v}_A^{\text{ext}}(t)}. \quad (74b)$$

According to (73) and (74), one has

$$\mathbf{z}_B^{\text{ext}}(t) = \mathbf{y}, \quad (75a)$$

$$\mathbf{v}_B^{\text{ext}}(t) = \sigma^2(t)\mathbf{1}. \quad (75b)$$

In addition, EM is implemented to update σ^2 as $\sigma^2(t+1)$. By setting

$$\tilde{\mathbf{y}}(t+1) = \mathbf{z}_B^{\text{ext}}(t), \quad (76a)$$

$$\tilde{\sigma}^2(t+1) = \mathbf{v}_B^{\text{ext}}(t) = \sigma^2(t)\mathbf{1}, \quad (76b)$$

we run the VALSE (noise variance aware) algorithm, and calculate $\mathbf{z}_A^{\text{post}}(t+1)$ and $\mathbf{v}_A^{\text{post}}(t+1)$. Then $\mathbf{z}_A^{\text{ext}}(t+1)$ and $\mathbf{v}_A^{\text{ext}}(t+1)$ are updated as

$$\frac{1}{\mathbf{v}_A^{\text{ext}}(t+1)} = \frac{1}{\mathbf{v}_A^{\text{post}}(t+1)} - \frac{1}{\tilde{\sigma}^2(t+1)}, \quad (77a)$$

$$\frac{\mathbf{z}_A^{\text{ext}}(t+1)}{\mathbf{v}_A^{\text{ext}}(t+1)} = \frac{\mathbf{z}_A^{\text{post}}(t+1)}{\mathbf{v}_A^{\text{post}}(t+1)} - \frac{\tilde{\mathbf{y}}(t+1)}{\tilde{\sigma}^2(t+1)}. \quad (77b)$$

According to (73), (75), (76) and (77), (72) is obtained. \blacksquare

According to Property 2, $\mathbf{v}_B^{\text{post}}(t+1) = \mathbf{v}_A^{\text{post}}(t+1)$ and $\mathbf{z}_B^{\text{post}}(t+1) = \mathbf{z}_A^{\text{post}}(t+1)$ holds when $\sigma^2(t) = \sigma^2(t+1)$, which means that the noise variance is a constant during the iteration. Combing Property 1 and Property 2, it is concluded that in the unquantized setting VALSE-EP is equivalent to VALSE when the noise variance is known, i.e., the noise variance estimation step is removed. In general, VALSE-EP is not exactly equivalent to VALSE even in the unquantized setting.

VII. NUMERICAL SIMULATION

In this section, numerical experiments are conducted to evaluate the performance of the proposed VALSE-EP algorithm. In addition, for performance comparison in the quantized setting, the AQNM is adopted and \mathbf{y}_q (69) is directly input to the VALSE to perform estimation. Furthermore, VALSE-EP is also compared with VALSE in unquantized setting.

A. Simulation Setup

The frequencies are randomly drawn such that the minimum wrap around distance is greater than $2\pi/N$. The noninformative prior, i.e., $p(\theta_i) = 1/(2\pi)$, $i = 1, \dots, N$, is used for both VALSE and VALSE-EP algorithm. The magnitudes of the weight coefficients are drawn i.i.d. from a Gaussian distribution $\mathcal{N}(1, 0.04)$, and the phases are drawn i.i.d. from a uniform distribution between $[-\pi, \pi]$. For multi-bit quantization, a uniform quantizer is adopted and the quantization interval is restricted to $[-3\sigma_z/\sqrt{2}, 3\sigma_z/\sqrt{2}]$, where σ_z^2 is the variance of \mathbf{z} . In our setting, it can be calculated that $\sigma_z^2 \approx K$. For one-bit quantization, zero is chosen as the threshold. The SNR is defined as $\text{SNR} = 20\log(\|\mathbf{A}(\boldsymbol{\theta})\mathbf{w}\|_2/\|\boldsymbol{\epsilon}\|_2)$. Both VALSE and VALSE-EP stop at iteration t if $\|\hat{\mathbf{z}}(t) - \hat{\mathbf{z}}(t-1)\|_2/\|\hat{\mathbf{z}}(t)\|_2 < 10^{-6}$ or the number of iterations exceeds 1000.

The signal estimation error $\text{NMSE}(\hat{\mathbf{z}})$, the frequency estimation error $\text{MSE}(\hat{\boldsymbol{\theta}})$ and the correct model order estimation probability $P(\hat{K} = K)$ are used to characterize the performance. The normalized MSE (NMSE) of signal $\hat{\mathbf{z}}$ (for unquantized and multi-bit quantized system) and MSE of $\hat{\boldsymbol{\theta}}$ are defined as $\text{NMSE}(\hat{\mathbf{z}}) \triangleq 10\log(\|\hat{\mathbf{z}} - \mathbf{z}\|_2^2/\|\mathbf{z}\|_2^2)$ and $\text{MSE}(\hat{\boldsymbol{\theta}}) \triangleq 10\log(\|\hat{\boldsymbol{\theta}} - \boldsymbol{\theta}\|_2^2)$, respectively. Please note that, due to magnitude ambiguity, it is impossible to recover the exact magnitude of \tilde{w}_k from one-bit measurements in the noiseless scenario. Thus for one-bit quantization, the debiased NMSE of the signal defined as $\text{dNMSE}(\hat{\mathbf{z}}) \triangleq \min_c 10\log(\|\mathbf{z}^* - c\hat{\mathbf{z}}\|_2^2/\|\mathbf{z}^*\|_2^2)$ is calculated. As for the frequency estimation error, we average only the trials in which all those algorithms estimate the correct model order. All the results are averaged over 500 Monte Carlo (MC) trials unless stated otherwise. The MSE of the frequency estimation is calculated only when the model order is correctly estimated.

At first, an experiment is conducted to show that VALSE-EP is able to suppress the harmonics coming from the quantized data. The parameters are set as follows: $N = 100$, $K = 2$ and the true frequencies are $\tilde{\boldsymbol{\theta}} = [-1, 2]^T$. The results are shown in Fig. 4 for $\text{SNR} = 0$ dB, $\text{SNR} = 20$ dB and $\text{SNR} = 40$ dB. As stated in [57], the one-bit data consists of plentiful harmonics including self-generated and cross-generated harmonics. especially at high SNR. For low SNR scenario ($\text{SNR} = 0$ dB), both VALSE and VALSE-EP estimate the model order successfully. For medium ($\text{SNR} = 20$ dB) and high SNR ($\text{SNR} = 40$ dB) scenario, VALSE overestimates the model order, outputs the fundamental (true) frequency and the

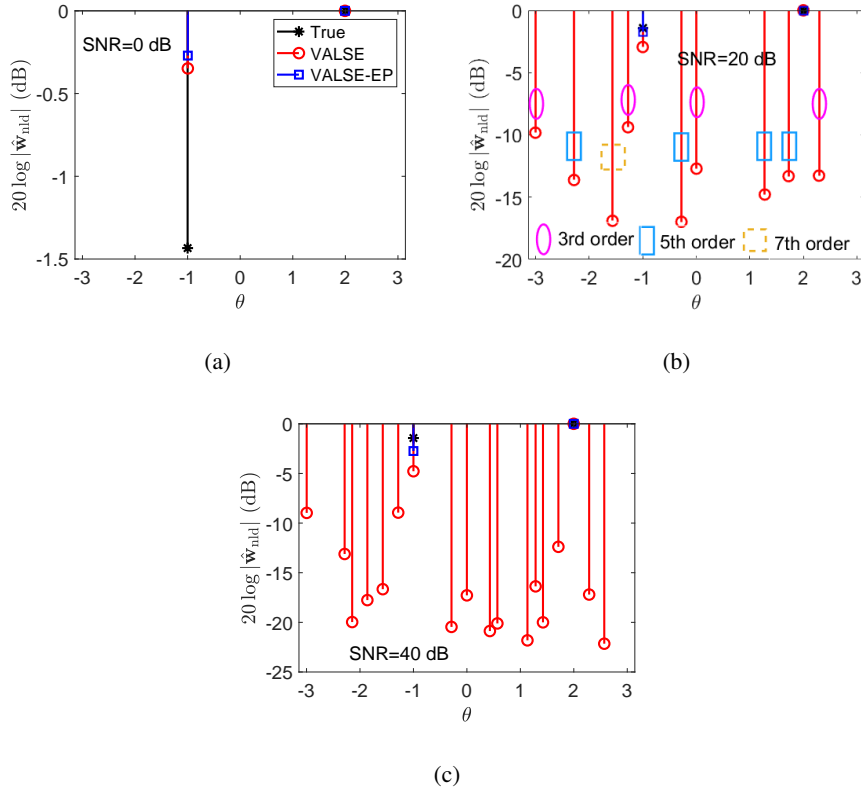


Fig. 4. A typical reconstruction results of VALSE-EP and VALSE under 1 bit quantization at SNR = 0 dB, SNR = 20 dB and SNR = 40 dB. The normalized amplitudes $\hat{\mathbf{w}}_{\text{nld}} \triangleq \hat{\mathbf{w}}/(\max_i |\hat{w}_i|)$ are plotted.

self-generated and cross-generated harmonics. For example, the 3rd order harmonics corresponding to $\mathcal{W}(-\theta_1 - 2\theta_2) \approx -3$, $\mathcal{W}(-\theta_1 + 2\theta_2) \approx -1.28$, $\mathcal{W}(2\theta_1 - \theta_2) \approx 2.29$, $\mathcal{W}(-2\theta_1 - \theta_2) = 0$, the 5th order harmonics corresponding to $\mathcal{W}(-4\theta_1 + \theta_2) \approx -0.28$, $\mathcal{W}(5\theta_1) \approx 1.28$, $\mathcal{W}(-2\theta_1 + 3\theta_2) \approx 1.72$, $\mathcal{W}(2\theta_1 + 3\theta_2) \approx -2.28$, the 7th order harmonic $\mathcal{W}(-3\theta_1 + 4\theta_2) \approx -1.57$, are estimated for SNR = 20 dB. While, VALSE-EP estimates the model order correctly for both SNR = 20 dB and SNR = 40 dB, demonstrating the effectiveness of suppressing the harmonics.

For the ensuing subsections, four numerical experiments with synthetic data and one with real data are conducted to demonstrate the excellent performance of VALSE-EP under quantized setting, compared to VALSE.

B. NMSE of the Line Spectral versus Iteration

The NMSEs of the reconstructed line spectral versus the iteration are investigated and results are shown in Fig. 5. Note that both VALSE-EP and VALSE converge in tens of iterations. For low SNR scenario (SNR = 0 dB), VALSE-EP and VALSE are comparable. As SNR increases, the performance gap between

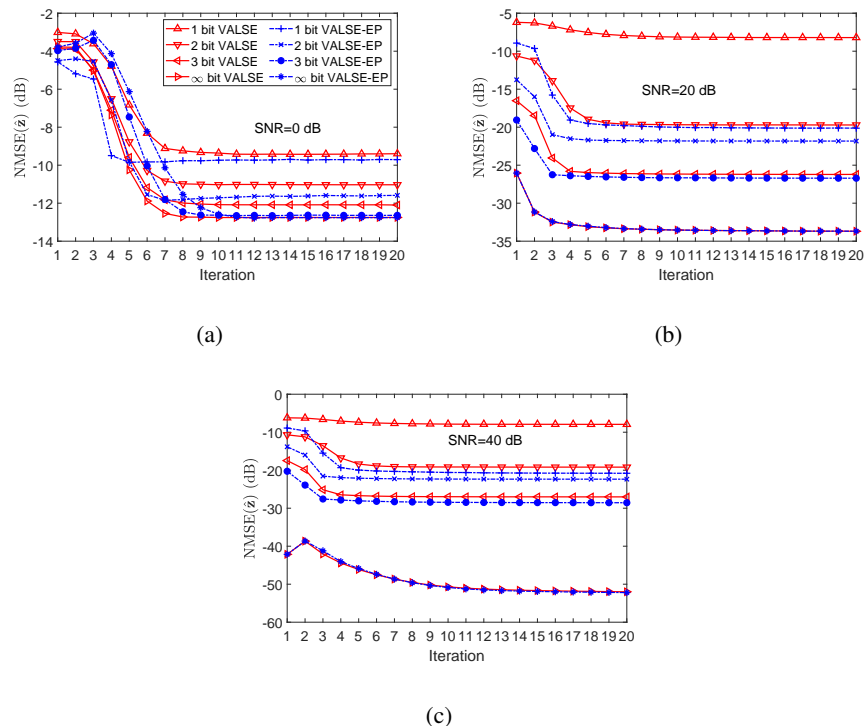


Fig. 5. The NMSE of the LSE of the VALSE-EP versus the number of iterations under SNR = 0 dB, SNR = 20 dB, SNR = 40 dB, respectively. Here $N = 100$ and $K = 3$.

VALSE-EP and VALSE increases under quantized settings. Besides, the performance of the VALSE-EP improves as SNR increases, especially for higher bit-depth. In contrast, for 1 bit quantization, VALSE works well under low SNR scenario, and degrades as SNR increases. As the bit-depth increases, the performances of the VALSE-EP and VALSE improve and approach to the unquantized setting.

C. Estimation versus SNR

The performance of the VALSE-EP versus SNR is investigated and the results are plotted in Fig. 6. For the signal reconstruction and model order estimation probability, Fig. 6(a) and 6(b) show that for 1 bit and 2 bit quantization, as SNR increases, the performances of VALSE first improve, and then degrade, while the performances of VALSE-EP always improve and are better than VALSE. A surprising phenomenon is that VALSE-EP under 2 bit quantization achieves the highest success rate of model order estimation and approaches to the CRB firstly. As the SNR continuous to increase, VALSE-EP deviates a little away from CRB under 1 bit and 2 bit quantization, while in the unquantized setting, both VALSE and VALSE-EP approach to the CRB asymptotically.

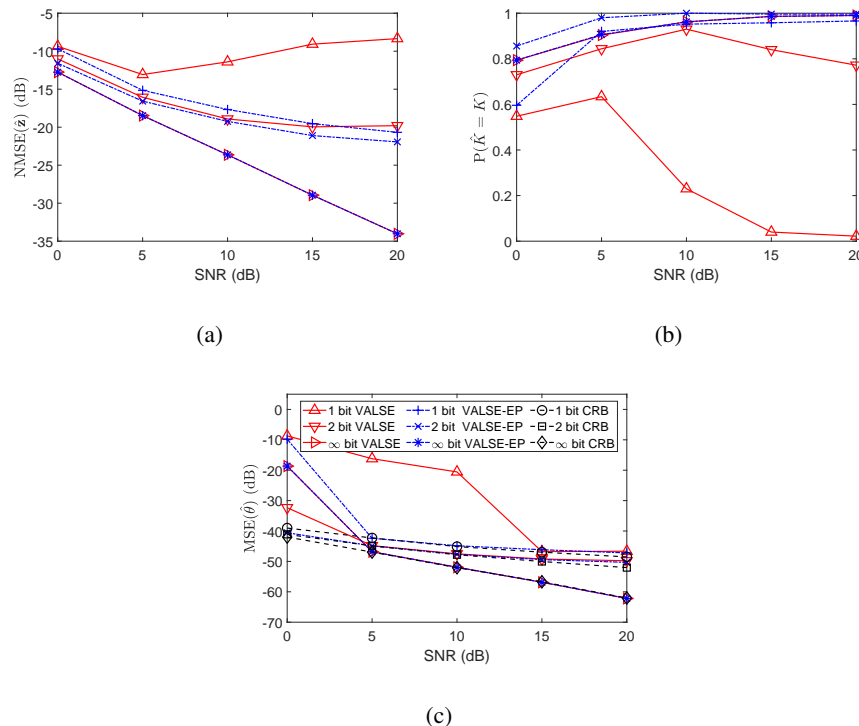


Fig. 6. Performance versus SNR for $N = 100$ and $K = 3$: (a) NMSE of the reconstructed signal; (b) success rate of model order estimation; (3) MSE of frequency estimation.

D. Estimation versus Number of Measurements N

The performances of both VALSE-EP and VALSE versus the number of measurements N are examined and results are shown in Fig. 7. For both algorithms, the signal reconstruction error decreases as the number of measurements N increases. It can be seen that VALSE-EP works better than VALSE under 1 bit and 2 bit quantization. As N increases, the success rate of model order estimation of VALSE first increases and then decreases under 1 bit quantization. In contrast, the success rate of model order estimation of VALSE-EP increases and even exceed the VALSE and VALSE-EP under unquantized setting for $N = 100$. As for the frequency estimation error, VALSE-EP approaches to the CRB quickly than VALSE under quantized setting.

E. Estimation versus Number of Spectral K

The performance of VALSE-EP is investigated with respect to the number of spectral K , and results are presented in Fig. 8. For the signal reconstruction error and success rate of model order estimation, the performances of all algorithms degrade as K increases, except that VALSE under 1 bit quantization, which first improves and then degrades. For the frequency estimation error, as K increases, VALSE

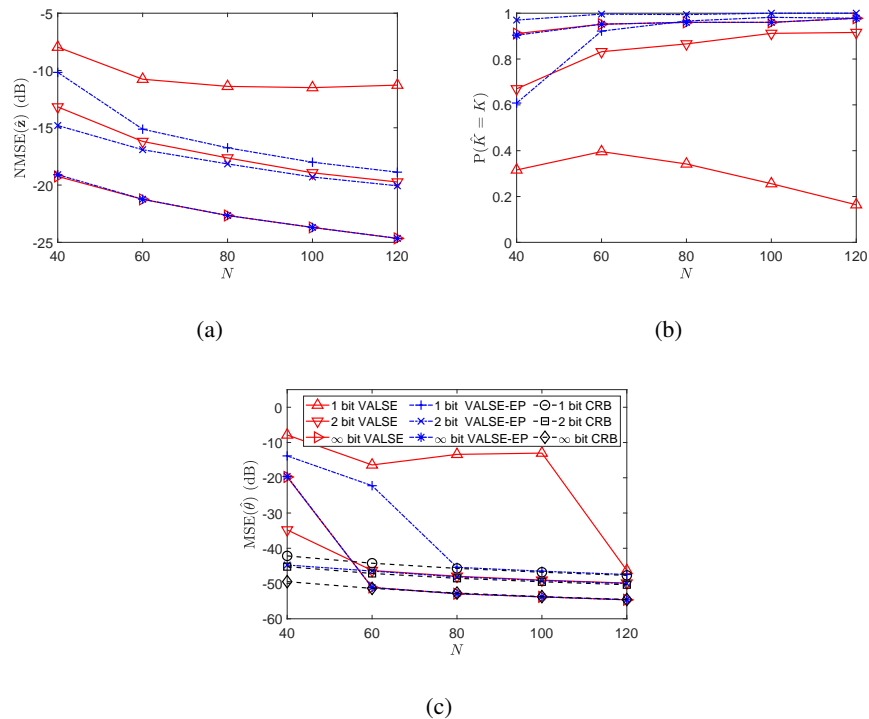


Fig. 7. The performance of VALSE-EP versus the number of measurements N for SNR = 10 dB and $K = 3$: (a) NMSE of the reconstructed signal; (b) success rate of model order estimation; (3) MSE of frequency estimation.

degrades quickly and deviates far way from CRB when $K \geq 4$ under 1 bit quantization. When $K \leq 6$, VALSE-EP is always close to the CRB under 1 bit quantization. As K continues to increase, the frequency estimation error of VALSE-EP begin to deviate far way from CRB.

F. Real Data

The performance of VALSE-EP is evaluated with real data collected at sea, which was collected on a HLA (part of the Shark array) during the Shallow Water 2006 (SW06) experiment on August 5 and 6, 2006 [58]. The array had 32 elements uniformly spaced at $d = 15$ m (design frequency $f = 50$ Hz, thus the wavelength λ is $\lambda = c/f = 1500/50 = 30$ m and $d = \lambda/2$). The first 1000 snapshots (8494 snapshots in total) are used. The source depths are estimated to be around 12 m. For the DOA problem, $\theta_i = -2\pi d/\lambda \sin \varphi_i = -\pi \sin \varphi_i$, where $\{\varphi_i\}_{i=1}^K$ denote the DOAs. The variance of the real data is calculated to be 0.0136, which is used to design the 2 bit quantizer.

The synthesized posterior PDF of frequencies $1/|\hat{\mathcal{S}}| \sum_{i=1}^{|\hat{\mathcal{S}}|} q(\theta_i | \mathbf{Y})|_{\theta_i = -\pi \sin \varphi_i}$ based on the data from one of the oblique runs is presented. In [58], it is stated that the towed source signal is at $\sin \varphi_1 \approx 0.1$, and a signal (the interferer source) near the endfire direction ($\sin \varphi_2 \approx -0.9$) is assumed to be from a ship

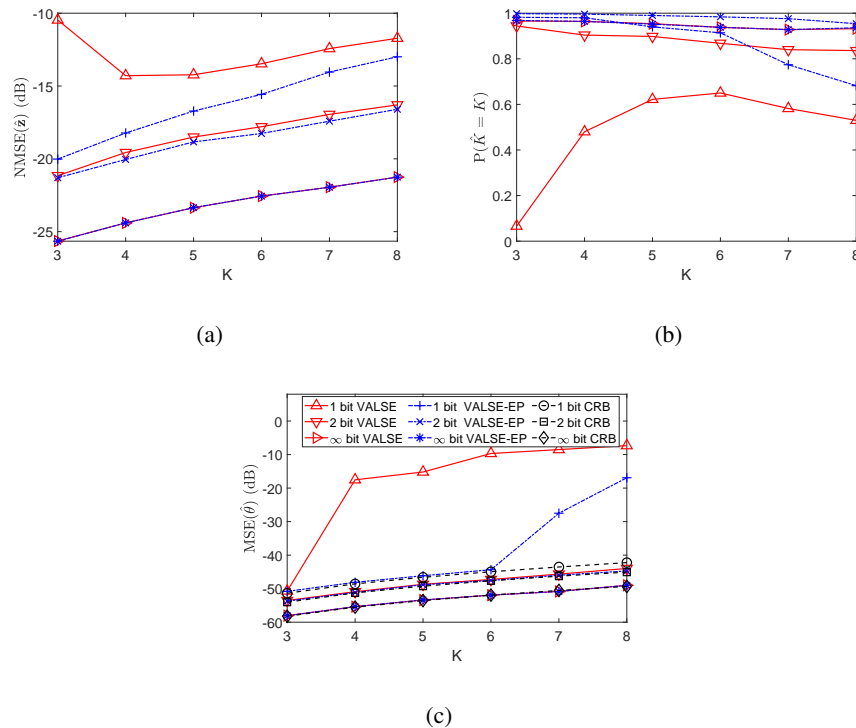


Fig. 8. The performance of VALSE-EP versus the number of spectrum K for $N = 160$ and $\text{SNR} = 10$ dB.

(The existence of this ship is unknown). For unquantized setting, Fig.9(c) and Fig. 9(f) are consistent with the results obtained in [58]. While when the data is heavily quantized into 1 bit and 2 bit, the towed source signal is estimated accurately and the interferer source disappears for VALSE-EP. In contrast, the towed source signal are estimated accurately for VALSE algorithm, with an additional false source signal corresponding to the third order harmonic $-3 \times (-\pi \sin \varphi_1) \approx 0.3\pi$ (located at -0.3 in Fig. 9(a)) of the fundamental frequency $-\pi \sin \varphi_1 \approx -0.1\pi$.

VIII. CONCLUSION

In this paper, a VALSE-EP algorithm is proposed to deal with the fundamental LSE problem from quantized samples. The VALSE-EP is one kind of low-complexity grid-less algorithm which iteratively refines the frequency estimates, automatically estimates the model order, and learns the parameters of the prior distribution and noise variance. Importantly, VALSE-EP provides the uncertain degrees of the frequency estimates from quantized samples. Substantial numerical experiments are conducted to show the excellent performance of the VALSE-EP, including on a real data set.

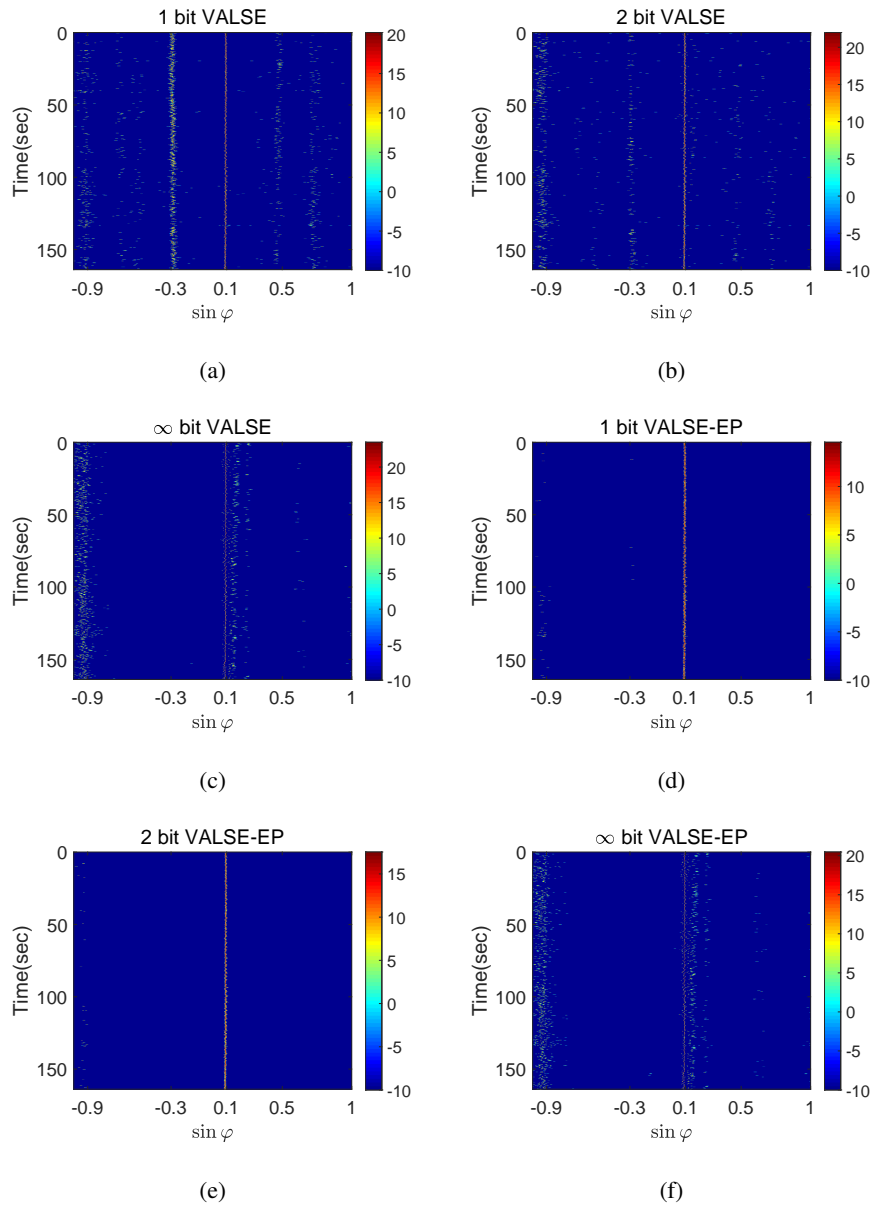


Fig. 9. The synthesized posterior PDF of $\sin \varphi$ for real data.

IX. ACKNOWLEDGEMENT

The authors acknowledge the editor and the four anonymous reviewers for valuable comments and suggestions on this work.

X. APPENDIX

A. Finding the local maximum of $\ln Z(\mathbf{s})$

A greedy iterative search strategy similar to [20] is adopted to find a local maximum of $\ln Z(\mathbf{s})$. We proceed as follows: In the p th iteration, the k th test sequence \mathbf{t}_k which flips the k th element of $\mathbf{s}^{(p)}$ is obtained. Then $\Delta_k^{(p)} = \ln Z(\mathbf{t}_k) - \ln Z(\mathbf{s}^{(p)})$ is calculated for each $k = 1, \dots, N$. If $\Delta_k^{(p)} < 0$ holds for all k , the algorithm is terminated and $\hat{\mathbf{s}}$ is set as $\mathbf{s}^{(p)}$, otherwise t_k corresponding to the maximum $\Delta_k^{(p)}$ is chosen as $\mathbf{s}^{(p+1)}$ in the next iteration.

When $k \notin \mathcal{S}$, that is, $s_k = 0$, we activate the k th component of \mathbf{s} by setting $s_k = 1$. Now, $\mathcal{S}' = \mathcal{S} \cup \{k\}$.

$$\begin{aligned} \Delta_k &= \ln Z(\mathbf{s}') - \ln Z(\mathbf{s}) \\ &= \ln \det(\mathbf{J}_{\mathcal{S}} + \frac{1}{\tau} \mathbf{I}_{|\mathcal{S}|}) - \ln \det(\mathbf{J}_{\mathcal{S}'} + \frac{1}{\tau} \mathbf{I}_{|\mathcal{S}'|}) \\ &\quad + \ln \frac{\rho}{1-\rho} + \ln \frac{1}{\tau} + \mathbf{h}_{\mathcal{S}'}^H (\mathbf{J}_{\mathcal{S}'} + \frac{1}{\tau} \mathbf{I}_{|\mathcal{S}'|})^{-1} \mathbf{h}_{\mathcal{S}'} - \mathbf{h}_{\mathcal{S}}^H (\mathbf{J}_{\mathcal{S}} + \frac{1}{\tau} \mathbf{I}_{|\mathcal{S}|})^{-1} \mathbf{h}_{\mathcal{S}}. \end{aligned} \quad (78)$$

Let \mathbf{j}_k be $\mathbf{j}_k = [J_{ik} | i \in \mathcal{S}]^T$. By using the block-matrix determinant formula, one has

$$\ln(\det(\mathbf{J}_{\mathcal{S}'} + \frac{1}{\tau} \mathbf{I}_{|\mathcal{S}'|})) = \ln \det(\mathbf{J}_{\mathcal{S}} + \frac{1}{\tau} \mathbf{I}_{|\mathcal{S}|}) + \ln \left(\text{tr}(\boldsymbol{\Sigma}^{-1}) + \frac{1}{\tau} - \mathbf{j}_k^H (\mathbf{J}_{\mathcal{S}} + \frac{1}{\tau} \mathbf{I}_{|\mathcal{S}|})^{-1} \mathbf{j}_k \right), \quad (79)$$

By the block-wise matrix inversion formula, one has

$$\mathbf{h}_{\mathcal{S}'}^H (\mathbf{J}_{\mathcal{S}'} + \frac{1}{\tau} \mathbf{I}_{|\mathcal{S}'|})^{-1} \mathbf{h}_{\mathcal{S}'} = \mathbf{h}_{\mathcal{S}}^H (\mathbf{J}_{\mathcal{S}} + \frac{1}{\tau} \mathbf{I}_{|\mathcal{S}|})^{-1} \mathbf{h}_{\mathcal{S}} + \frac{\xi^* \xi}{\text{tr}(\boldsymbol{\Sigma}^{-1}) + \frac{1}{\tau} - \mathbf{j}_k^H (\mathbf{J}_{\mathcal{S}} + \frac{1}{\tau} \mathbf{I}_{|\mathcal{S}|})^{-1} \mathbf{j}_k}, \quad (80)$$

where $\xi = h_k - \mathbf{j}_k^H (\mathbf{J}_{\mathcal{S}} + \frac{1}{\tau} \mathbf{I}_{|\mathcal{S}|})^{-1} \mathbf{h}_{\mathcal{S}}$. Plugging (79) and (80) in (78), and let

$$\begin{aligned} v_k &= \left(\text{tr}(\boldsymbol{\Sigma}^{-1}) + \frac{1}{\tau} - \mathbf{j}_k^H (\mathbf{J}_{\mathcal{S}} + \frac{1}{\tau} \mathbf{I}_{|\mathcal{S}|})^{-1} \mathbf{j}_k \right)^{-1} \quad \text{and} \\ u_k &= v_k \left(h_k - \mathbf{j}_k^H (\mathbf{J}_{\mathcal{S}} + \frac{1}{\tau} \mathbf{I}_{|\mathcal{S}|})^{-1} \mathbf{h}_{\mathcal{S}} \right), \end{aligned} \quad (81)$$

Δ_k can be simplified as

$$\Delta_k = \ln \frac{v_k}{\tau} + \frac{|u_k|^2}{v_k} + \ln \frac{\rho}{1-\rho}. \quad (82)$$

Given that \mathbf{s} is changed into \mathbf{s}' , the mean $\hat{\mathbf{w}}'_{\mathcal{S}'}$ and covariance $\hat{\mathbf{C}}'_{\mathcal{S}'}$ of the weights can be updated from (40), i.e.,

$$\hat{\mathbf{C}}'_{\mathcal{S}'} = (\mathbf{J}_{\mathcal{S}'} + \frac{1}{\tau} \mathbf{I}_{|\mathcal{S}'|})^{-1}, \quad (83a)$$

$$\hat{\mathbf{w}}'_{\mathcal{S}'} = \hat{\mathbf{C}}'_{\mathcal{S}'} \mathbf{h}_{\mathcal{S}'}. \quad (83b)$$

In fact, the matrix inversion can be avoided when updating $\hat{\mathbf{w}}'_{S'}$ and $\hat{\mathbf{C}}_{S'}$. It can be shown that

$$\begin{aligned} & \begin{pmatrix} \hat{\mathbf{C}}'_{S' \setminus k} & \hat{\mathbf{c}}'_k \\ \hat{\mathbf{c}}_k^H & \hat{C}'_{kk} \end{pmatrix} = (\mathbf{J}_{S'} + \frac{1}{\tau} \mathbf{I}_{|S'|})^{-1} \\ & = \begin{pmatrix} \hat{\mathbf{C}}_S & \mathbf{0} \\ \mathbf{0} & 0 \end{pmatrix} + v_k \begin{pmatrix} \hat{\mathbf{C}}_S \mathbf{j}_k \\ -1 \end{pmatrix} \begin{pmatrix} \hat{\mathbf{C}}_S \mathbf{j}_k \\ -1 \end{pmatrix}^H = \begin{pmatrix} \hat{\mathbf{C}}_S + v_k \hat{\mathbf{C}}_S \mathbf{j}_k (\hat{\mathbf{C}}_S \mathbf{j}_k)^H & -v_k \hat{\mathbf{C}}_S \mathbf{j}_k \\ -v_k (\hat{\mathbf{C}}_S \mathbf{j}_k)^H & v_k \end{pmatrix} \end{aligned} \quad (84)$$

$\hat{\mathbf{C}}'_{S'}$ is obtained if $\hat{\mathbf{c}}'_k$, $\hat{\mathbf{c}}_k^H$ and \hat{C}'_{kk} are inserted appropriately in $\hat{\mathbf{C}}'_{S' \setminus k}$, and

$$\begin{aligned} & \begin{pmatrix} \hat{\mathbf{w}}'_{S' \setminus k} \\ \hat{w}'_k \end{pmatrix} = \hat{\mathbf{C}}_{S'} \mathbf{h}_{S'} \\ & = \begin{pmatrix} \hat{\mathbf{C}}_S \mathbf{h}_S + v_k \hat{\mathbf{C}}_S \mathbf{j}_k \mathbf{j}_k^H \hat{\mathbf{C}}_S \mathbf{h}_S - v_k \hat{\mathbf{C}}_S \mathbf{j}_k h_k \\ -v_k \mathbf{j}_k^H \hat{\mathbf{C}}_S \mathbf{h}_S + v_k h_k \end{pmatrix} = \begin{pmatrix} \hat{\mathbf{C}}_S \mathbf{h}_S - u_k \hat{\mathbf{C}}_S \mathbf{j}_k \\ u_k \end{pmatrix}. \end{aligned} \quad (85)$$

From (85) and (84), one can see that after activating the k th component, the posterior mean and variance of w_k are u_k and v_k , respectively.

For the deactive case with $s_k = 1$, $s'_k = 0$ and $S' = S \setminus \{k\}$, $\Delta_k = \ln Z(s') - \ln Z(s)$ is the negative of (82), i.e.,

$$\Delta_k = -\ln \frac{v_k}{\tau} - \frac{|u_k|^2}{v_k} - \ln \frac{\rho}{1-\rho}. \quad (86)$$

Similar to (84), the posterior mean and covariance update equation from S' to S case can be rewritten as

$$\begin{pmatrix} \hat{\mathbf{C}}'_{S'} & \mathbf{0} \\ \mathbf{0} & 0 \end{pmatrix} + v_k \begin{pmatrix} \hat{\mathbf{C}}'_{S'} \mathbf{j}_k \\ -1 \end{pmatrix} \begin{pmatrix} \hat{\mathbf{C}}'_{S'} \mathbf{j}_k \\ -1 \end{pmatrix}^H = \begin{pmatrix} \hat{\mathbf{C}}_{S \setminus k} & \hat{\mathbf{c}}_k \\ \hat{\mathbf{c}}_k^H & \hat{C}_{kk} \end{pmatrix}, \quad (87)$$

and

$$\begin{pmatrix} \hat{\mathbf{w}}'_{S'} - u_k \hat{\mathbf{C}}'_{S'} \mathbf{j}_k \\ u_k \end{pmatrix} = \begin{pmatrix} \hat{\mathbf{C}}'_{S'} \mathbf{h}_{S'} - u_k \hat{\mathbf{C}}'_{S'} \mathbf{j}_k \\ u_k \end{pmatrix} = \begin{pmatrix} \hat{\mathbf{w}}_{S \setminus k} \\ \hat{w}_k \end{pmatrix}, \quad (88)$$

where $\hat{\mathbf{c}}_{k,0}$ denotes the column of $\hat{\mathbf{C}}_{S,0}$ corresponding to the k th component. According to (87) and (88), one has

$$\hat{\mathbf{C}}'_{S'} + v_k \hat{\mathbf{C}}'_{S'} \mathbf{j}_k \mathbf{j}_k^H \hat{\mathbf{C}}'_{S'} = \hat{\mathbf{C}}_{S \setminus k}, \quad (89a)$$

$$-v_k \hat{\mathbf{C}}'_{S'} \mathbf{j}_k = \hat{\mathbf{c}}_k \quad (89b)$$

$$v_k = \hat{C}_{kk}, \quad (89c)$$

$$\hat{\mathbf{w}}'_{S'} - u_k \hat{\mathbf{C}}'_{S'} \mathbf{j}_k = \hat{\mathbf{w}}_{S \setminus k}, \quad (89d)$$

$$u_k = \hat{w}_k. \quad (89e)$$

Thus, $\hat{\mathbf{C}}'_{S'}$ can be updated by substituting (89b) and (89c) in (89a), i.e.,

$$\hat{\mathbf{C}}'_{S'} = \hat{\mathbf{C}}_{S \setminus k} - v_k \hat{\mathbf{C}}'_{S'} \mathbf{j}_k \mathbf{j}_k^H \hat{\mathbf{C}}'_{S'} = \hat{\mathbf{C}}_{S \setminus k} - \frac{\hat{\mathbf{c}}_k \hat{\mathbf{c}}_k^H}{\hat{C}_{kk}}. \quad (90)$$

Similarly, $\hat{\mathbf{w}}'_{S'}$ can be updated by substituting (89b) and (89e) in (89d), i.e.,

$$\hat{\mathbf{w}}'_{S'} = u_k \hat{\mathbf{C}}'_{S'} \mathbf{j}_k + \hat{\mathbf{w}}_{S \setminus k} = \hat{\mathbf{w}}_{S \setminus k} - \frac{\hat{w}_k}{\hat{C}_{kk}} \hat{\mathbf{c}}_k. \quad (91)$$

According to $v_k = \hat{C}_{kk}$ (89c) and $u_k = \hat{w}_k$ (89e), Δ_k (86) can be simplified as

$$\Delta_k = -\ln \frac{\hat{C}_{kk}}{\tau} - \frac{|w_k|^2}{\hat{C}_{kk}} - \ln \frac{\rho}{1 - \rho}. \quad (92)$$

B. Calculating the post variance $\mathbf{v}_A^{\text{post}}$ (64) of \mathbf{z}

Now we calculate the variance of z_n given $q(\mathbf{w}_{\hat{S}}|\tilde{\mathbf{y}})$ and $q(\boldsymbol{\theta}|\tilde{\mathbf{y}})$. Let $\mathbf{b}_n^T = [e^{j(n-1)\theta_1}, e^{j(n-1)\theta_2}, \dots, e^{j(n-1)\theta_K}]$ be the n th row of $\mathbf{A}_{\hat{S}}$. Then $z_n = \mathbf{b}_n^T \mathbf{w}_{\hat{S}}$. The variance is

$$\begin{aligned} \text{Var}[z_n] &= \text{E}[|z_n|^2] - |\text{E}[z_n]|^2 = \text{E}[|\mathbf{b}_n^T \mathbf{w}_{\hat{S}}|^2] - |\text{E}[\mathbf{b}_n^T \mathbf{w}_{\hat{S}}]|^2 \\ &= \text{tr} \left[(\mathbf{C}_{\hat{S}} + \hat{\mathbf{w}}_{\hat{S}} \hat{\mathbf{w}}_{\hat{S}}^H) \text{E}[\mathbf{b}_n^* \mathbf{b}_n^T] \right] - |\hat{\mathbf{b}}_n^T \hat{\mathbf{w}}_{\hat{S}}|^2. \end{aligned} \quad (93)$$

where

$$\text{E}[\mathbf{b}_n^* \mathbf{b}_n^T] = \hat{\mathbf{b}}_n^* \hat{\mathbf{b}}_n^T + \text{diag} \left(\mathbf{1}_{\hat{K}} - |\hat{\mathbf{b}}_n|^2 \right). \quad (94)$$

Substituting (94) in (93), one obtains (64).

REFERENCES

- [1] VALSE-EP code, <https://github.com/RiverZhu/VALSE-EP>
- [2] W. Bajwa, A. Sayeed, and R. Nowak, "Compressed channel sensing: A new approach to estimating sparse multipath channels," *Proc. IEEE*, vol. 98, pp. 1058-1076, Jun. 2010.
- [3] B. Ottersten, M. Viberg and T. Kailath, "Analysis of subspace fitting and ML techniques for parameter estimation from sensor array data," *IEEE Trans. Signal Process.*, vol. 40, pp. 590-600, 1992.
- [4] P. Stoica and R. L. Moses, *Spectral Analysis of Signals*. Upper Saddle River, NJ, USA: Prentice-Hall, 2005.
- [5] R. Schmidt, "Multiple emitter location and signal parameter estimation," *IEEE Trans. Antennas Propag.*, vol. 34, no. 3, pp. 276-280, 1986.
- [6] R. Roy and T. Kailath, "ESPRIT-estimation of signal parameters via rotational invariance techniques," *IEEE Trans. Acoust., Speech, Signal Process.*, vol. 37, no. 7, pp. 984-995, 1989.
- [7] Z. Yang Z, J. Li, P. Stoica P and Xie L, "Sparse methods for direction-of-arrival estimation," *Academic Press Library in Signal Processing*, vol. 7, pp. 509-581, 2018.

- [8] D. Malioutov, M. Cetin and A. Willsky, "A sparse signal reconstruction perspective for source localization with sensor arrays," *IEEE Trans. Signal Process.*, vol. 53, no. 8, pp. 3010-2022, 2005.
- [9] Y. Chi, L. L. Scharf, A. Pezeshki and R. Calderbank, "Sensitivity of basis mismatch to compressed sensing," *IEEE Trans. on Signal Process.*, vol. 59, pp. 2182 - 2195, 2011.
- [10] B. Mamandipoor, D. Ramasamy and U. Madhow, "Newtonized orthogonal matching pursuit: Frequency estimation over the continuum," *IEEE Trans. Signal Process.*, vol. 64, no. 19, pp. 5066-5081, 2016.
- [11] J. Fang, F. Wang, Y. Shen, H. Li and R. S. Blum, "Superresolution compressed sensing for line spectral estimation: an iterative reweighted approach," *IEEE Trans. Signal Process.*, vol. 64, no. 18, pp. 4649-4662, 2016.
- [12] T. L. Hansen, B. H. Fleury and B. D. Rao, "Superfast line spectral estimation," *IEEE Trans. Signal Process.*, vol. 66, no. 10, pp. 2511-2526, 2018.
- [13] L. Hu, J. Zhou, Z. Shi and Q. Fu, "A fast and accurate reconstruction algorithm for compressed sensing of complex sinusoids," *IEEE Trans. Signal Process.*, vol. 61, no. 22, pp. 5744-5754, 2013.
- [14] L. Hu, Z. Shi, J. Zhou and Q. Fu, "Compressed sensing of complex sinusoids: An approach based on dictionary refinement," *IEEE Trans. Signal Process.*, vol. 60, no. 7, pp. 3809-3822, 2012.
- [15] G. Tang, B. Bhaskar, P. Shah and B. Recht, "Compressed sensing off the grid," *IEEE Trans. Inf. Theory*, vol. 59, no. 11, pp. 7465-7490, 2013.
- [16] Z. Yang and L. Xie, "On gridless sparse methods for line spectral estimation from complete and incomplete data," *IEEE Trans. Signal Process.*, vol. 63, no. 12, pp. 3139-3153, 2015.
- [17] Y. Li and Y. Chi, "Off-the-grid line spectrum denoising and estimation with multiple measurement vectors," *IEEE Trans. Signal Process.*, vol. 64, no. 5, pp. 1257-1269, 2016.
- [18] Z. Yang, L. Xie and C. Zhang, "A discretization-free sparse and parametric approach for linear array signal processing," *IEEE Trans. Signal Process.*, vol. 62, no. 19, pp. 4959-4973, 2014.
- [19] S. Boyd and L. Vandenberghe, *Convex Optimization*, Cambridge University Press, 2004.
- [20] M. A. Badiu, T. L. Hansen and B. H. Fleury, "Variational Bayesian inference of line spectra," *IEEE Trans. Signal Process.*, vol. 65, no. 9, pp. 2247-2261, 2017.
- [21] J. Zhu, Q. Zhang, P. Gerstoft, M. A. Badiu and Z. Xu, "Grid-less variational Bayesian line spectral estimation with multiple measurement vectors," *Signal Process.*, vol. 61, pp. 155-164, 2019.
- [22] S. Rangan, T. S. Rappaport and E. Erkip, "Millimeter-wave cellular wireless networks: potentials and challenges," *Proc. IEEE*, vol. 102, no. 3, pp. 366-385, 2014.
- [23] O. Mehanna and N. Sidiropoulos, "Frugal sensing: Wideband power spectrum sensing from few bits," *IEEE Trans. on Signal Process.*, vol. 61, no. 10, pp. 2693-2703, 2013.

- [24] Y. Chi and H. Fu, "Subspace learning from bits," *IEEE Trans. on Signal Process.*, vol. 65, no. 17, pp. 4429-4442, Sept 2017.
- [25] P. Schniter and S. Rangan, "Compressive phase retrieval via generalized approximate message passing," *IEEE Trans. Signal Process.*, vol. 63, no. 4, pp. 1043-1055, 2015.
- [26] S. Wang, L. Zhang and X. Jing, "Phase retrieval motivated nonlinear MIMO communication with magnitude measurements," *IEEE Trans. Wireless Commun.*, vol. 16, no. 8, pp. 5452-5466, 2017.
- [27] F. Li, J. Fang, H. Li and L. Huang, "Robust one-bit Bayesian compressed sensing with sign-flip errors," *IEEE Signal Process. Lett.*, vol. 22, no. 07, 2015.
- [28] J. Fang, Y. Shen, L. Yang and H. Li, "Adaptive one-bit quantization for compressed sensing," *Signal Process.*, vol. 125, pp. 145-155, 2016.
- [29] G. Franceschetti, V. Pascazio, G. Schirinzi, "Processing of signum coded SAR signal: theory and experiments," *IEE Proceedings F - Radar and Signal Processing*, vol. 138, no. 3, pp. 192-198, 1991.
- [30] C. Gianelli, L. Xu, J. Li, P. Stoica, "One-bit compressive sampling with time-varying thresholds for sparse parameter estimation," *IEEE Sensor Array and Multichannel Signal Processing Workshop (SAM)*, Rio de Janeiro, Brazil, July 10-13, 2016.
- [31] J. Li, M. M. Naghsh, S. J. Zahabi, M. M. Hashemi, "compressive radar sensing via one-bit sampling with time-varying thresholds," *50th Asilomar Conference on Signals, Systems and Computers*, Pacific Grove, CA, USA, 6-9 Nov. 2016.
- [32] K. Yu, Y. Zhang, M. Bao, Y. Hu and Z. Wang, "DOA estimation from one-bit compressed array data via joint sparse representation," *IEEE Signal Process. Lett.*, vol. 23, no. 9, pp. 1279-1283, 2016.
- [33] X. Meng, J. Zhu, "A generalized sparse Bayesian learning algorithm for one-bit DOA estimation," *IEEE Commun. Lett.*, vol. 22, no. 7, pp. 1414-1417, 2018.
- [34] Y. Gao, D. Hu, Y. Chen, Y. Ma, "Gridless 1-b DOA estimation exploiting SVM approach," *IEEE Commun. Lett.*, vol. 21, no. 10, pp. 2210-2213, 2017.
- [35] C. Gianelli, L. Xu, J. Li, P. Stoica, "One-bit compressive sampling with time-varying thresholds for multiple sinusoids," *IEEE 7th International Workshop on Computational Advances in Multi-Sensor Adaptive Processing (CAMSAP)*, 10-13 Dec. 2017, Curacao, Netherlands Antilles.
- [36] C. Li, R. Zhang, J. Li and P. Stocia, "Bayesian information criterion for signed measurements with application to sinusoidal signals," *IEEE Signal Process. Lett.*, vol. 25, no. 8, pp. 1251-1255, 2018.
- [37] C. Zhou, Z. Zhang, F. Liu, B. Li, "Gridless compressive sensing method for line spectral estimation from 1-bit measurements," *Digital Signal Processing*, vol. 60, pp. 152-162, 2017.
- [38] H. Fu and Y. Chi, "Quantized spectral compressed sensing: Cramér-Rao bounds and recovery algorithms," *IEEE Trans. Signal Process.*, vol. 66, no. 12, pp. 3268-3279, 2018.

- [39] C. J. Wang, C. K. Wen, S. Jin, S. H. Tsai, “Gridless channel estimation for mixed one-bit antenna array systems,” *IEEE Trans. Wireless Commun.*, vol. 17, no. 12, pp. 8485-8501, 2018.
- [40] T. Minka, “A family of algorithms for approximate Bayesian inference,” Ph.D. dissertation, Department of Electrical Engineering and Computer Science, Mass. Inst. Technol., Cambridge, MA, USA, 2001.
- [41] X. Meng, S. Wu and J. Zhu, “A unified Bayesian inference framework for generalized linear models,” *IEEE Signal Process. Lett.*, vol. 25, no. 3, pp. 398-402, 2018.
- [42] J. Zhu, L. Han and X. Meng, “An AMP-based low complexity generalized sparse Bayesian learning algorithm,” *IEEE Access*, vol. 7, pp. 7965-7976, 2018.
- [43] Y. A. Kabashima, “CDMA multiuser detection algorithm on the basis of belief propagation,” *Journal of Physics A: Mathematical and General*, vol. 36, no. 43, 2003.
- [44] D. L. Donoho, A. Maleki, and A. Montanari, “Message passing algorithms for compressed sensing: I. Motivation and construction” in *Proc. Inf. Theory Workshop*, Cairo, Egypt, Jan. 2010, pp. 1-5.
- [45] X. Meng, S. Wu, L. Kuang, and J. Lu, “An expectation propagation perspective on approximate message passing,” *IEEE Signal Process. Lett.*, vol. 22, no. 8, pp. 1194-1197, Aug. 2015.
- [46] S. Wu, L. Kuang, Z. Ni, J. Lu, D. Huang, and Q. Guo, “Low-complexity iterative detection for large-scale multiuser MIMO-OFDM systems using approximate message passing,” *IEEE J. Sel. Topics Signal Process.*, vol. 8, no. 5, pp. 902-915, May 2014.
- [47] S. Rangan, “Generalized approximate message passing for estimation with random linear mixing,” in *Proc. IEEE Int. Symp. Inf. Theory*, Jul. 2011, pp. 2168-2172.
- [48] S. Rangan, P. Schniter, and A. Fletcher, “Vector approximate message passing,” arXiv preprint arXiv:1610.03082, 2016.
- [49] P. Schniter, S. Rangan, and A. K. Fletcher, “Vector approximate message passing for the generalized linear model,” in *Proc. 50th Asilomar Conf. Signals, Syst. Comput.*, Nov. 2016, pp. 1525-1529.
- [50] D. P. Wipf and B. D. Rao, “Sparse Bayesian learning for basis selection,” *IEEE Trans. Signal Process.*, vol. 52, no. 8, pp. 2153-2164, 2004.
- [51] X. Meng and J. Zhu, “Bilinear adaptive generalized vector approximate message passing,” *IEEE Access*, vol. 7, pp. 4807-4815, 2018.
- [52] K. V. Mardia and P. E. Jupp, *Directional Statistics*. New York, NY, USA: Wiley, 2000.
- [53] K. P. Murphy, *Machine Learning: A Probabilistic Perspective*. MIT Press, 2012.
- [54] Bertsekas, D. P. and Tsitsiklis : *Parallel and Distributed Computation: Numerical Methods*, Athenan Scientific: Massachusetts, 1997.
- [55] M. E. Rasekh and U. Madhow, “Noncoherent compressive channel estimation for mm-wave massive

- MIMO,” *52nd Asilomar Conference on Signals, Systems, and Computers*, 2018.
- [56] A. Zymnis, S. Boyd and E. Candès, “Compressed sensing with quantized measurements,” *IEEE Signal Process. Lett.*, vol. 17, no. 2, pp. 149-152, 2010.
- [57] B. Jin, J. Zhu, Q. Wu, Y. Zhang and Z. Xu, “One-bit LFM CW radar: spectrum analysis and target detection,” arXiv preprint, arXiv:1905.09440.
- [58] T. C. Yang, “Deconvolved conventional beamforming for a horizontal line array,” *IEEE J. Oceanic Eng.*, vol. 43, no. 1, pp. 160-172, 2018.
- [59] J. P. Vila and P. Schniter, “Expectation-maximization Gaussian-mixture approximate message passing,” *IEEE Trans. Signal Process.*, vol. 61, no. 19, pp. 4658-4672, 2013.